HHS Public Access

Author manuscript

Mol Cell. Author manuscript; available in PMC 2022 December 16.

Published in final edited form as:

Mol Cell. 2021 December 16; 81(24): 4979–4993.e7. doi:10.1016/j.molcel.2021.10.026.

Parp1 promotes sleep, which enhances DNA repair in neurons

David Zada[1], **Yaniv Sela**[2], **Noa Matosevich**[2], **Adir Monsonego**[1], **Tali Lerer-Goldshtein**[1], **Yuval Nir**[2], **Lior Appelbaum**[1,3,*]

[1]The Faculty of Life Sciences and the Multidisciplinary Brain Research Center, Bar-Ilan University, Ramat-Gan, 5290002, Israel.

[2]Department of Physiology and Pharmacology, Sackler Faculty of Medicine, and Sagol School of Neuroscience, Tel Aviv University, Tel Aviv-Yafo 69978, Israel.

[3]Lead contact

Summary

The characteristics of the sleep drivers and the mechanisms through which sleep relieves the cellular homeostatic pressure are unclear. In flies, zebrafish, mice, and humans, DNA damage levels increase during wakefulness and decrease during sleep. Here, we showed that 6 h of consolidated sleep is sufficient to reduce DNA damage in the zebrafish dorsal pallium. Induction of DNA damage by neuronal activity and mutagens triggered sleep and DNA repair. The activity of the DNA damage response (DDR) proteins Rad52 and Ku80 increased during sleep, and chromosome dynamics enhanced Rad52 activity. The activity of the DDR initiator poly ADP-ribose polymerase 1 (Parp1) increased following sleep deprivation. In both larva zebrafish and adult mice, Parp1 promoted sleep. Inhibition of Parp1 activity reduced sleep-dependent chromosome dynamics and repair. These results demonstrate that DNA damage is a homeostatic driver for sleep, and Parp1 pathways can sense this cellular pressure and facilitate sleep and repair activity.

Graphical Abstract

*Corresponding author: lior.appelbaum@biu.ac.il.

Author contributions

DZ and LA conceived and designed the experiments. DZ performed the molecular, imaging, behavioral experiments, and data analysis. TLG performed immunohistochemistry experiments, western blot, and cloning. DZ and AM established transgenic lines. YS, NM, DZ, and YN designed mouse experiments. YS and NM performed and analyzed mouse experiments, with supervision from YN. YN, YS. and NM wrote mice-relevant manuscript sections. DZ and LA prepared the figures and wrote the paper with feedback from all authors.

Declaration of Interests

The authors declare no conflict of interests.

Supplemental Information in Supplementary File.

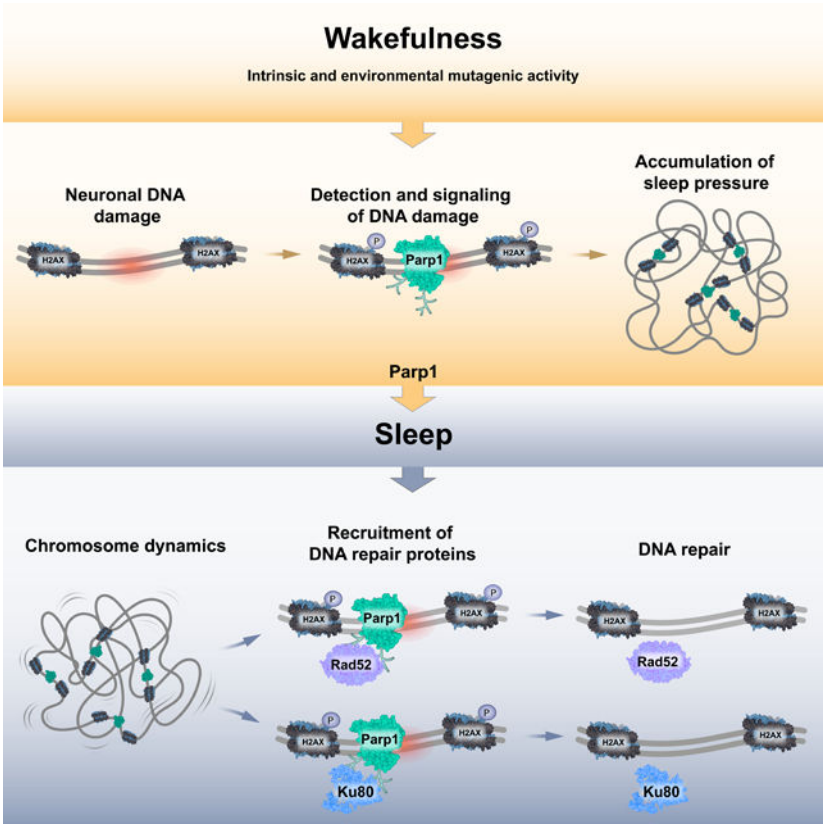

eTOC blurb

The cellular processes that benefit from sleep and the mechanisms driving sleep regulation remain unclear. Zada et al. report that buildup of DNA damage in neurons during wakefulness increases sleep pressure. Parp1 senses DNA damage and promotes sleep, which facilitates efficient DNA repair and reduction of the cellular homeostatic pressure.

Keywords

Sleep; homeostasis; DNA damage response; Rad52; Ku80; Parp1; zebrafish; mice; chromosome dynamics; NREM

Introduction

Sleep, accompanied by reduced responsiveness to external stimuli, is a vulnerable behavioral state. However, sleep is evolutionary conserved across phylogeny, and all studied animals with neural networks, including jellyfish, worms, mollusks, flies, fish, reptiles, birds, rodents, and humans, require sleep (Joiner, 2016; Keene and Duboue, 2018). Sleep disturbances can cause neural impairment and are associated with neurodevelopmental and neurodegenerative diseases and aging (Carroll et al., 2016; Sabia et al., 2021). Although sleep is essential for all animals, the daily amount of sleep varies significantly between species (Allada and Siegel, 2008). While adult humans sleep approximately 7–8 hours per day (Hirshkowitz et al., 2015), the owl monkey sleeps 17 hours (Sri Kantha et al., 2009), and

free-roaming wild elephants sleep only 2 hours (Gravett et al., 2017). These diverse sleep requirements raise fundamental questions: what dictates a species-specific sufficient amount of sleep, and what is the restorative neural process?

The timing, duration, and quality of sleep are regulated by an interaction between the circadian clock and homeostatic sleep pressure, which builds up during extended wakefulness (Borbély, 1982). Homeostatic factors are thought to accumulate with increasing duration and intensity of wakefulness prior to sleep (Allada et al., 2017; Eban-Rothschild et al., 2017; Weber and Dan, 2016). However, the cellular homeostatic mechanisms that drive sleep need, and the identity of the homeostatic factors, are unclear. Extensive research has suggested various possibilities, including accumulation of toxic metabolites (Xie et al., 2013), increased cellular need for energy, supplies, and macromolecules (Mackiewicz et al., 2007), and increased synaptic number and strength (Tononi and Cirelli, 2014), as well as elevated neural damage (Singh and Donlea, 2020; Stanhope et al., 2020) and cellular stress (Hill et al., 2014; Lenz et al., 2015).

Enriched wakefulness and neuronal activity induce DNA double-strand breaks (DSBs) in mice and flies (Bellesi et al., 2016; Madabhushi et al., 2015; Suberbielle et al., 2013). The repair of DNA lesions in neurons is slower than in dividing cells (Barzilai et al., 2008), suggesting that lesions can be accumulated during wakefulness. Indeed, we have demonstrated that DSBs accumulate in the neurons of zebrafish larvae while they are awake. In contrast, sleep increases chromosome dynamics that can reduce the levels of DNA damage in neurons (Zada et al., 2019). Similarly, sleep deprivation (SD) can increase DNA damage and decrease the expression of DNA repair genes in human blood cells (Carroll et al., 2016; Cheung et al., 2019). These studies suggest that sleep promotes nuclear maintenance, i.e. sleep regulates the balance between DNA damage and repair. Nevertheless, it remains unclear whether the formation of DNA damage is inhibited, or the activity of the repair systems is more stimulated, during sleep.

Elucidating the underlying mechanisms that associate sleep, DNA damage, and repair is challenging. In *Caenorhabditis elegans*, stress-induced sleep is promoted by CEP-1, a member of the DNA damage response (DDR) pathway (DeBardeleben et al., 2017). The DDR comprises four main pathways: homologous recombination (HR), non-homologous end joining (NHEJ), base excision repair (BER), and nucleotide excision repair (NER). Each involves a different combination of repair proteins that are sequentially recruited into the damaged site (Jackson and Bartek, 2009). One of the first events in the DDR, which is common to all pathways, is the recruitment of poly (ADP-ribose) polymerase-1 (PARP-1) to the damage site. PARP-1 is a detector of DNA damage and promotes the accumulation of downstream DDR proteins (Ray Chaudhuri and Nussenzweig, 2017). These nuclear proteins can be used as markers to identify repair in a specific genomic locus and to distinguish between the diverse pathways (Polo and Jackson, 2011). For example, RAD52 and RAD51 are active in the DSB resection process, which is a critical step in HR but not in the NHEJ repair process. The KU70/KU80 heterodimer binds the DNA ends and then recruits and activates additional factors in the NHEJ pathway (Polo and Jackson, 2011). In contrast, the APEX1 protein initiates the BER process (Vidal et al., 2001), while the DDB2 protein participates in the NER process, which is the main DNA repair mechanism activated after

exposure to ultraviolet (UV) radiation (Stoyanova et al., 2009). Elucidating whether and how sleep regulates DDR pathways in individual neurons can provide information about its beneficial cellular function and explain the cause for variability in the duration of restorative sleep.

Here, we utilized the transparent zebrafish to identify cellular sleep drivers and understand the role of sleep in the restoration of nuclear homeostasis in single neurons of live vertebrates. The zebrafish is a well-established sleep model (Zhdanova et al., 2001; Prober et al., 2006; Yokogawa et al., 2007; Zada and Appelbaum, 2020), and the structure and function of its brain, as well as the DNA damage and repair systems, are conserved with mammals (Pei and Strauss, 2013; Leung et al., 2013; Cayuela et al., 2018; Gerlai, 2020). Recently, brain-wide activity recording has revealed two major sleep signatures in the dorsal pallium (DP) of the zebrafish larvae. These states, named slow bursting sleep (SBS) and propagating wave sleep (PWS), closely resemble mammalian slow-wave sleep (SWS) and rapid eye movement/paradoxical sleep (REM/PS), respectively (Leung et al., 2019). In this study, a combination of behavioral monitoring and live imaging of the dynamic clustering of DNA repair proteins under manipulations of sleep, neuronal activity, and DNA damage and repair revealed that DNA damage in neurons is a homeostatic driver for sleep. Furthermore, Parp1 can induce sleep, which promotes chromosome dynamics and the recruitment and activity of DDR proteins.

Results

Six hours of consolidated sleep is sufficient to normalize neuronal DNA damage

Exposure to light during the night promotes wakefulness in diurnal animals, including zebrafish and humans (Yokogawa et al., 2007; Lockley et al., 2006). In order to find the minimal consolidated sleep period required to reduce homeostatic sleep pressure, we monitored sleep in 5–7 days post-fertilization (dpf) larvae during two consecutive days, where the length of the first night was truncated. As expected, under the baseline 14 h light/10 h dark (LD) conditions, sleep time (minutes/hour) increased 5.3-fold during the night (Figure 1A, B, B`). During the truncated dark period of 2 and 4 h of the first night (zeitgeber time ZT14-ZT16 and ZT14-ZT18), sleep time increased 5.8-fold and 5.9-fold, respectively. Nonetheless, the larvae kept sleeping during the remaining time of the subjective night as well as 3 and 2 h, respectively, of the day (Figure 1C, C`, D, D', G). The extended periods of sleep in the light following the short dark period demonstrate that 2 or 4 h of sleep are not sufficient to significantly reduce the homeostatic sleep pressure. In contrast, a significant sleep rebound was not observed when the night dark period was extended to 6 h (ZT14-ZT20, Figure 1E, E`, G) and 8 h (ZT14-ZT22, Figure 1F, F`, G). Notably, in the 2 and 4 h dark period experiments, although sleep rebound was apparent during the subjective night and the following recovery period during the day, the rebound sleep time per hour was lower than during a standard dark night (Figure 1C, C`, D, D`). In addition, the quality of sleep was compromised as a result of a decrease in sleep/wake transitions and sleep bout length, and an increase in wake bout length compared to a standard dark night (Table S1). Nevertheless, by ZT4 on the following day, all groups had slept for an amount of time (2 h: 275.13 ± 10.93 min, 4 h: 234.87 ± 12.56 min, 6 h: 254.75 ± 9.41 min, and 8 h: 261.5 ± 15.13

min) that was comparable to the standard 10 h night (275.16 ± 14.81 min). Furthermore, the sleep/wake cycle of the 2nd day was normal, and sleep increased similarly during the night in all groups (Figure 1A–F). This indicates that the light manipulations during the first night did not shift the rhythmic sleep/wake cycle. The results demonstrate that a minimum of 6 h of consolidated sleep during the night is sufficient for the larvae to dissipate their homeostatic sleep pressure.

Which cellular process set the level of the homeostatic pressure to sleep? We have previously demonstrated that DNA damage accumulates in the larval neurons during wakefulness and decreases during nighttime sleep (Zada et al., 2019). These changes in DNA damage were confirmed using the comet assay (Figure S1A, B), and were not detected in other cell types (Figure S1C–F). Accordingly, we used the γH2AX marker to examine whether 6 h of consolidated sleep during the night is sufficient to normalize the levels of DNA damage. We focused on neurons within the DP, which demonstrate slow synchronous bursts of activity during sleep (Leung et al., 2019), and whose average activity is reduced during sleep compared to wakefulness in larvae (Figure S2). The levels of DNA damage in single neurons of the DP of 5–6 dpf larvae were quantified during the day (ZT4 and ZT14), the night (following the dark period at either ZT16, ZT18, ZT20, ZT22, or ZT0), and the following day (ZT4 and ZT14). By the end of the daytime wake period (5 dpf, ZT14), there was approximately twice the number of γH2AX foci than at the beginning of the day under both LD and constant dark conditions (5 dpf, ZT4, Figure 1J–N, Figure S1G, H). Under LD, the number of γH2AX foci returned to baseline levels by the end of the 10 h nighttime sleep in DP neurons (ZT0, Figure 1J). In contrast, the number of γH2AX foci remained unchanged or was only slightly reduced after 2 h (ZT16, Figure 1K) and 4 h (ZT18, Figure 1L), of sleep, respectively, compared to the end of the wake period (ZT14). Analysis of the levels of DNA damage at the end of the sleep rebound period (ZT4) exhibited by the sleep deprived larvae (Figure 1C, D) indicated that the numbers of γH2AX foci had returned to normal levels at ZT4 (Figure 1K, L). In contrast to these sleep deprived animals (Figure 1C, D), larvae that had slept at least 6 h in nighttime darkness were able to lower the levels of γH2AX foci in their neurons to normal (ZT20, ZT22, Figure 1M, N), as was the case in the control group (Figure 1J). Recapitulating the changes during the first monitored day (5 dpf), the number of γH2AX foci increased by approximately 2-fold by the end of the daytime wakefulness period in all groups of 6 dpf larvae (Figure 1J–N). Likewise, in the wake-promoting noradrenergic neurons of the locus coeruleus (Hayat et al., 2020), the number of γH2AX foci increased toward the end of the day (ZT14) and reduced during the end of the night (ZT0) in 6 dpf *tg(dbh:Gal4/uas:EGFP)* larvae (Figure S1I, J). These results indicate that a minimum of 6 h of consolidated nighttime sleep can counteract the DNA damage accumulated during wakefulness in non-dividing mature neurons. Furthermore, even though a shorter consolidated sleep period in the dark is insufficient to reduce DNA damage, a period of sleep rebound in the light can restore the normal low levels of DNA damage. Altogether, these results suggest that homeostatic sleep pressure is driven by the accumulation of neuronal DNA damage, which can be reduced during recovery sleep.

Induction of DNA damage by neuronal activity or by UV radiation promotes sleep

Sleep correlates with normalization of the levels of DNA damage (Figure 1). Since there is evidence that DNA damage can be induced by neuronal activity in mice (Madabhushi et al., 2015; Suberbielle et al., 2013), we examined whether stimulation of neuronal activity would increase DNA damage and sleep pressure. During daytime wakefulness, 6 dpf larvae were treated for 30 minutes with pentylenetetrazole (PTZ), which induces robust brain-wide neuronal activity (Reichert et al., 2019). The numbers of γH2AX foci were quantified following the PTZ treatment to verify that the induced neuronal activity affects DNA damage (Figure 2A). As expected, the number of γH2AX foci in neurons of the DP increased immediately following PTZ treatment and reduced to normal levels 3 h post-treatment (Figure 2B). Monitoring sleep behavior revealed that sleep time increased by 5-fold 1 h post-PTZ treatment and remained elevated during the next 3 h (Figure 2C). Normal wakefulness and complete recovery were observed 5 h after PTZ treatment (Figure 2C).

Considering that PTZ affects cell activity in the whole larvae and has additional effects such as seizures (Baraban et al., 2005), the channel-rhodopsin 2 (ChR2) was used to directly modulate neuronal activity. DNA damage and sleep time were quantified pre- and post-optogenetic stimulation in neurons of live larvae. This was achieved by exposing 6 dpf ChR2+ [*tg(HuC:Gal4/uas:ChR2-mCherry)*] (Helmbrecht et al., 2018) and ChR2− sibling larvae [*tg(HuC:Gal4)* or *tg(uas:ChR2-mCherry)* or WT] to 10 minutes of repeated alternating blue light pulses. The number of γH2AX foci in neurons of the DP of the ChR2+ larvae increased by approximately 3.5-fold 1 h after the stimuli and returned to baseline after 3 h, with no change in the ChR2− siblings (Figure 2D and E). Validating the induction of DNA damage by neuronal activity, the comet assay showed that blue light stimuli increased the tail moment in neurons extracted from ChR2+ brains (Figure S1B). In accordance, while both ChR2+ and ChR2− groups presented with the same basal sleep levels, the sleep time of the ChR2+ larvae increased approximately 2-fold during 3 h following the stimuli (Figure 2F). These results show that neuronal activity increases DNA damage, which promotes sleep.

Neuronal DNA damage can be induced by a variety of cellular processes (Barzilai et al., 2008), and is not solely linked to increased cell activity. If DNA damage indeed drives homeostatic sleep pressure, then additional intrinsic and extrinsic factors affecting DNA damage would be expected to increase the pressure to sleep, independently of neuronal activity. Therefore, we exposed the larvae to UV radiation, which damages DNA (Sinha and Häder, 2002). Immunohistochemical analysis with an antibody against phosphorylated-ERK (pERK), a well-established reporter of neuronal activity (Randlett et al., 2015), verified that the levels of pERK in neurons of the DP of 6 pdf larvae were not elevated following UV treatment (Figure 2G). In order to understand whether UV radiation affects DNA damage and sleep, we exposed 6 dpf larvae to 2 min of 5–10 mW/cm^2 UV radiation (302 nm) during the day (ZT5). The number of γH2AX foci increased 30 min post-exposure and peaked 30 min later (Figure 2H), while sleep increased and remained elevated for 2 h (Figure 2I, Figure S3). Both sleep time and the number of γH2AX foci returned to normal levels after 3 h (Figure 2H, I). In line with our previous observations on sleep triggered by a chemical

mutagen (Zada et al., 2019), the results demonstrate that even in the absence of induced neuronal activity, an increase in the levels of DNA damage promotes sleep, which can normalize the levels of DNA damage.

Sleep increases the activity of the repair proteins Rad52 and Ku80

How can sleep reduce DNA damage in neurons, and which proteins are required to achieve this effect? The lowering of the levels of DNA damage during sleep could either reflect a lower rate of DNA breakage, or an increase in the rate and efficiency of repair. In order to study DNA repair, we tested the expression levels of genes involved in various DDR pathways during the day, night and post SD. While the transcription of the DDR genes is predominantly controlled by the light/dark cycle, the transcription of *rad52* and *ku80* can also be regulated by homeostatic sleep pressure (Figure S4A–F). To study the kinetics of DDR protein assembly and disassembly at the site of DNA damage in neurons of live transgenic larvae, we fused the zebrafish Rad52 and Ku80 to fluorescent proteins and used the *HuC:Gal4/uas* system to express these markers for HR and NHEJ, respectively, in larval neurons (STAR Methods, Figure S4K–N). Similar fusion proteins have previously been used as DNA repair markers in human cell lines (Britton et al., 2013; Karanam et al., 2012). We imaged and quantified the number of Ku80-EGFP foci during the day and night, and post SD, in single neurons of 6 dpf *tg(HuC:Gal4)* larvae that transiently expressed the *pT2-uas:Ku80-EGFP* construct. The results revealed a low number of Ku80-EGFP foci during the day (ZT4) with an increase in foci during the night (ZT18, Figure 3A, B). Immediately following SD (ZT18), the number of Ku80-EGFP foci was lower in the sleep deprived larvae as compared to controls. However, over the following day (ZT4), after the sleep rebound, the number of Ku80-EGFP foci in the sleep deprived larvae increased to reach the normal nighttime levels seen in the control larvae (Figure 3B). These results demonstrate that sleep enhances the clustering and activity of Ku80 DNA repair proteins.

In order to continuously monitor DNA repair activity during the 24 h cycle and to test whether the sleep-dependent DNA repair activity also occurs in other repair pathways, we performed time-lapse imaging of DsRed-Rad52 foci in single neurons of the DP of 6 dpf *tg(HuC:Gal4/uas:DsRed-Rad52)* larvae during the day and night (Figure 3C, D). Similar to the Ku80-EGFP foci, the number of DsRed-Rad52 foci was low during the day and increased by about 2-fold during the night (Figure 3E, E’). Notably, the number of DsRed-Rad52 foci returned to the low levels typical of daytime wakefulness after 8 h of nighttime sleep (Figure 3E). In order to differentiate between sleep and a circadian effect, the 6 dpf *tg(HuC:Gal4/uas:DsRed-Rad52)* larvae were sleep-deprived for 4 h during the night (ZT14-ZT18). Immediately following SD (ZT18), the number of DsRed-Rad52 foci was low and resembled the levels observed during daytime wakefulness (Figure 3E, E’). During the sleep rebound period, the number of DsRed-Rad52 foci in the sleep deprived larvae increased and reached the nighttime levels of the control group. This number remained elevated during the night and the following 3 h of the subjective day and only returned to baseline levels after 9 h (Figure 3E). These results demonstrate the induction of Rad52 activity during sleep. Moreover, while the number of γH2AX foci was reduced after 6 h of consolidated sleep (Figure 1), 8–9 h were required for sleep-induced repair activity, suggesting that the upregulation of repair activity during sleep can continue during wakefulness.

Sleep is increased following the induction of DNA damage (Figure 1, 2). Since repair activity increased during sleep (Figure 3A–E`), the numbers of Ku80 and Rad52 foci were quantified following the PTZ treatment to examine whether the subsequent sleep period is associated with repair activity. There was no change in the numbers of DsRed-Rad52 foci in neurons of the DP of *tg(HuC:Gal4/uas:DsRed-Rad52)* larvae or the Ku80-EGFP foci in neurons of *pT2-uas:Ku80-EGFP*-injected *tg(HuC:Gal4)* larvae immediately post-treatment. However, 2 h into the recovery sleep period (Figure 2C), the numbers of both DsRed-Rad52 and Ku80-EGFP foci increased and remained elevated until 3 h post-treatment (Figure 3F, I). Since PTZ increases neuronal activity and does not directly cause damage in the DNA, we treated the larvae with UV radiation and Etoposide (ETO), which inhibits DNA topoisomerase II ligase activity and thereby generates DSBs (Tammaro et al., 2013). UV radiation of either DsRed-Rad52-positive neurons in the DP of *tg(HuC:Gal4/uas:DsRed-Rad52)* larvae or Ku80-EGFP-positive neurons in the brain of *pT2-uas:Ku80-EGFP*-injected *tg(HuC:Gal4)* larvae, upregulated the number of DsRed-Rad52 (Figure 3G), but not Ku80-EGFP foci (Figure 3J) when live imaging was conducted during 3 h following the exposure. The lack of change in the number of Ku80-EGFP foci is probably because the NHEJ pathway is less involved in the repair of UV damage (Sinha and Häder, 2002). Next, we monitored the effect of ETO treatment on DNA repair by live imaging of DsRed-Rad52 and Ku80-EGFP markers in individual larvae, before and after the treatment. Daytime ETO treatment of 6 dpf *tg(HuC:Gal4/uas:DsRed-Rad52)* or *pT2-uas:Ku80-EGFP*-injected *tg(HuC:Gal4)* larvae upregulated the numbers of both DsRed-Rad52 and Ku80-EGFP foci after 2 h (Figure 3H, K). Altogether, these results show that induction of DNA damage by either extended wakefulness, robust acute neuronal activity or mutagens increases sleep and upregulates the activity of repair pathways.

Chromosome dynamics promote Rad52 clustering

How does sleep facilitate the assembly of DDR proteins? One explanation could involve acceleration of chromosome dynamics and increased accessibility to damaged sites during sleep (Caridi et al., 2018; Tsouroula et al., 2016; Zada et al., 2019). In order to examine this possibility, we inhibited chromosome dynamics by overexpressing the lamina-associated polypeptide 2β [Lap2β, Figure 4A, B, (Zada et al., 2019)] that interacts with the chromatin and lamina and mediates their attachment to the inner- and intra-nuclear structures (Dechat et al., 2000; Prokocimer et al., 2009). To examine the effect of stable inhibition of chromosome dynamics on sleep, DNA damage, and repair in larvae and adults, a *tg(HuC:Gal4/uas:Lap2β-EGFP)* line (Lap2β-EGFP+) was established (Figure 4A, B). Larvae were treated with ETO, which induces DNA damage and recovery sleep (Zada et al., 2019). As expected, 2 h following ETO treatment, the chromosome dynamics increased by 2-fold in Lap2β-EGFP− neurons. In contrast, the chromosome dynamics remained low in Lap2β-EGFP+ neurons in the DP of *tg(HuC:Gal4/uas:Lap2β-EGFP/uas:DsRed-TRF1)* larvae (Figure 4C, D). To exclude toxic effect and validate that binding of Lap2β complex to the chromatin can inhibit chromosome dynamics, we deleted the LAP2-emerin-MAN1 (LEM)-domain, a motif that binds the chromatin-interacting protein barrier-to-autointegration factor (BAF) (Wagner and Krohne, 2007), and expressed the deleted Lap2β^{LEMdel}-EGFP protein in the larval neurons. As was observed in Lap2β-EGFP− neurons, 2 h following the ETO treatment, chromosome dynamics increased in

Lap2β^{LEMdel}-EGFP over-expressing neurons (Figure 4C, D). Next, this system was used to examine whether *Lap2β*-mediated inhibition of chromosome dynamics affects the activity of DDR proteins. The baseline number of DsRed-Rad52 foci was low during the day in neurons of the DP of *tg(HuC:Gal4/uas:Lap2β-EGFP/uas:DsRed-Rad52)* larvae (Figure 4E, F). When the repair system was challenged by treating the *tg(HuC:Gal4/uas:Lap2β-EGFP/uas:DsRed-Rad52)* larvae with ETO, the number of DsRed-Rad52 foci in the control Lap2β-EGFP− neurons increased 1.4-fold immediately after treatment and reached a 2-fold increase by 2 h post-treatment. In contrast, there was no rise in the number of DsRed-Rad52 foci in the Lap2β-EGFP+ neurons (Figure 4F). These results demonstrate that inhibition of chromosome dynamics impedes the efficient function of the Rad52 repair system. Accordingly, a sleep-mediated increase of chromosome dynamics can enable efficient repair activity.

Chronic inhibition of chromosome dynamics increases DNA damage and compensatory sleep

The next step was to test if chronic inhibition of chromosome dynamics and the repair machinery could affect neuronal DNA damage and alter the sleep/wake cycle. The levels of DNA damage in neurons was quantified in Lap2β-EGFP+ and their Lap2β-EGFP− sibling [*tg(HuC:Gal4)* or *tg(uas:Lap2β-EGFP)* or WT] larvae at 5 and 6 dpf, as well as 3 and 10 months post fertilization (mpf). As expected, *Lap2β*-mediated inhibition of chromosome dynamics and the repair system resulted in consistently increased numbers of γH2AX foci in neurons of the DP in Lap2β-EGFP+ zebrafish (Figure 4G). Intriguingly, sleep time increased during both day and night in Lap2β-EGFP+ larvae compared to their Lap2β-EGFP− sibling larvae (Figure 4H, H'). This increased sleep time was accompanied by lower neuronal activity in neurons of the DP of 6dpf Lap2β-EGFP+ larvae (Figure 4I, J). These results reinforce the notion that accumulation of neuronal DNA damage is not necessarily linked to increased neuronal activity, but that chronic inhibition of DNA repair proteins increases neuronal DNA damage and homeostatic sleep pressure, which promote sleep.

Parp1 increases sleep, chromosome dynamics, and the activity of Rad52

Sleep promotes the activity of DDR signaling pathways (Figure 3) that includes DNA damage sensors, signal transducers, and effector proteins (Harper and Elledge, 2007; Jackson and Bartek, 2009). Considering the rapidity of the sleep response to acute induction of DNA damage (Figure 2, 5, S3), we reasoned that activation of a DDR protein might signal the organism to sleep in order to increases chromosome dynamics and enable the efficient assembly of repair proteins. PARP-1 is a highly conserved DNA damage detector (Langelier and Pascal, 2013) and an organizer of the nuclear architecture in a way that facilitates DNA repair and cell survival in response to single- and double-strand DNA breaks (Beck et al., 2014; Pascal, 2018). To quantify the expression levels of Parp1 during sleep and wake, the mRNA and protein were extracted from WT larvae during the day, night, and following SD. While *parp1* mRNA expression levels were rhythmic and upregulated during the daytime (Figure S5A), the protein expression lagged behind and increased during the nighttime in the whole larvae (Figure S5B). To measure Parp1 activity and clustering on the chromatin specifically in the brain, rather than expression levels in the whole animal,

immunostaining was performed using Parp1 antibody (Figure 5A). The number of Parp1 foci increased during the day by 2.8-fold (ZT14 compared to ZT4) and normalized back to baseline levels by the end of the night (ZT0) in the nuclei of neurons in the DP. Following SD and the extended wakefulness (ZT18), the number of Parp1 foci reached higher levels than during natural wakefulness (ZT14) and sleep (ZT18). On the following subjective day, during the rebound sleep, the number of Parp1 foci reduced (Figure 5B). These results show that the activity of Parp1 in neurons is regulated by homeostatic sleep pressure.

To better understand the effect of Parp1 on sleep, we used an inducible heat shock promoter to overexpress Parp1 in a specific developmental stage. At ZT5, *pT2-hsp70:Parp1*-injected 6 dpf larvae were subjected to heat shock. Over-expression of Parp1, confirmed by immunoblotting (Figure S5C), increased sleep time by 1.7-fold in 6 dpf *pT2-hsp70:Parp1*-injected larvae compared to control *pT2-hsp70:Gal4*-injected sibling larvae during the day (Figure 5C, C`). These results demonstrate that Parp1 is sufficient to rapidly promote sleep. To test whether Parp1 is a required regulator of sleep, we knocked-down Parp1 (Parp1-KD) using the highly effective CRISPR/Cas9 system (Kroll et al., 2021). The knockdown strategy was selected because inherited Parp1 mutation in the whole larvae is expected to affect the embryo development. Indeed, Parp1 protein expression levels were reduced in Parp1-KD larvae (Figure S5C). In both Parp1-KD and control larvae, sleep time increased during the night compared to the day. Notably, sleep time was reduced during the end of the day, a period in which the homeostatic sleep pressure is built, and during the whole night in the Parp1-KD larvae (Figure 5D, D'). These results oppose the sleep phenotype observed in Parp1-overexpressing larvae and show that KD of Parp1 reduces sleep. Since Parp1 activity is increased in accordance with sleep pressure (Figure 5B), and to assess how Parp1 activity affects sleep, we inhibited Parp1 catalytic activity in 5–6 dpf larvae by using two doses (50, 100 μM) of the Parp1 inhibitor NU1025 (Bowman et al., 2001), and monitored sleep over two consecutive 14 h light/ 10 h dark cycles. The results revealed a dose-dependent reduction of sleep time during the night in NU1025-treated animals compared to DMSO-treated animals (Figure 5E, E'). Following withdrawal of the drug (ZT4), NU1025 larvae treated with both doses of NU1025 recovered and demonstrated transient increase (50 μM 1.8-fold; 100 μM 2.5-fold) of sleep time (Figure 5E, E'). All groups exhibited a similarly normal level of sleep time during the following day (Figure 5E, E'). Notably, NU1025 treatment did not show neuronal activity stimulating effect (Figure S5D). These results demonstrate that inhibition of Parp1 activity impedes sleep. Altogether, these experiments show that Parp1 is both a sufficient and necessary sleep regulator.

In order to examine the effect of Parp1 on daily changes in DNA damage, the number of γH2AX foci in neurons of the DP was monitored during and post NU1025 treatment. The number of γH2AX foci increased towards the end of the day in NU1025-treated larvae. Notably, the number of γH2AX foci was higher in NU1025-treated compared to control DMSO-treated larvae during day and night. This effect was particularly pronounced by the end of the night (ZT0, Figure 5F), whereas by the end of the treatment (ZT3), the number of γH2AX foci was 1.3- and 1.5-fold higher in the 50 and 100 μM NU1025-treated larvae, respectively, compared to the appropriate controls. Following the drug withdrawal and sleep rebound (ZT5), the number of γH2AX foci returned to normal levels (Figure 5F). These results show that Parp1 reduces DNA damage in the DP neurons and suggest that even

under intense DNA damage, NU1025-treated larvae do not sense the DNA damage-driven homeostatic sleep pressure.

While the number of γH2AX foci increased 30 min post UV radiation (Figure 2H), Parp1 protein expression increased immediately post UV radiation in larvae (Figure S5C). To test whether Parp1 activity is necessary to drive sleep-mediated chromosome dynamics and repair after induction of DNA damage, NU1025-treated larvae were exposed to UV radiation. As expected, sleep time in DMSO-treated larvae increased by approximately 4- and 2-fold, at 1 and 2 h post UV exposure, respectively, but there was no increase in NU1025-treated larvae (Figure 5G). In accordance with the sleep pattern, 2 h post UV exposure, in the neurons of the DP, chromosome dynamics increased by 1.75-fold in *tg(HuC:Gal4/uas:EGFP-Terfa)* DMSO-treated larvae (Figure 5H). The number of DsRed-Rad52 foci increased by ~2-fold in *tg(HuC:Gal4/uas:DsRed-Rad52)* DMSO-treated larvae (Figure 5I). In contrast, chromosome dynamics and the number of DsRed-Rad52 foci remained low 2 h post UV exposure in NU1025-treated larvae (Figure 5H, I). These results show that Parp1 activity promotes sleep and chromosome dynamics enabling efficient DNA repair.

In addition to UV radiation, various types of DNA damage inducers can promote sleep-dependent DNA repair, including neuronal activity (Figure 2, 3). Therefore, we examined the effect of Parp1 activity on sleep following optogenetic stimulation. As expected, DMSO-treated ChR2+ larvae increase sleep time by 2.3-, 2.8- and 2.5-fold, at 1, 2, and 3 h post blue light stimulation, respectively. However, sleep time did not increase in NU1025-treated ChR2+ larvae (Figure 5J). Furthermore, inhibition of the DNA repair activity resulted in increased DNA damage and compensatory sleep in Lap2β over-expressing larvae (Figure 4). To test whether inhibition of Parp1 activity can mask the drive to sleep even under chronic increased DNA damage, 6 dpf Lap2β-EGFP+ and their Lap2β-EGFP− sibling larvae were treated with 100 μM NU1025. Sleep time for all groups was longer at night than during the day and was reduced after treatment with NU1025. While sleep time was still longer in Lap2β-EGFP+ larvae compared to Lap2β-EGFP− sibling larvae, NU1025 treatment inhibited sleep in Lap2β-EGFP+ larvae (Figure 5K, K’). Altogether, these results show that inhibition of Parp1 can counteract the DNA damage-mediated signal to sleep, whether the stimulus is exposure to UV, mediated by neuronal activity, or spontaneous daytime and *Lap2β*-induced chronic sleep pressure. These data show that the DDR initiator Parp1 regulates the homeostatic drive to sleep.

Inhibition of Parp1 activity reduces NREM sleep duration and intensity in mice

To extend the findings in larva zebrafish to adult mammals with quantitative analysis of sleep depth, we tested how pharmacological inhibition of Parp1 affects sleep in adult male mice. Sleep monitoring was performed with gold-standard polysomnography including electroencephalogram (EEG), electromyogram (EMG) and video (Figure S6). Inspecting sleep/wake dynamics in the first few hours after drug delivery at light onset, revealed a 33 ± 10% reduction in NREM sleep 0.75 – 1.5 h following the administration of NU1025 compared with vehicle control (Figure 5L). During this temporal interval, less NREM sleep (more wakefulness) was clearly evident in individual subject data (Figure 5M). Moreover,

we observed that even when going above and beyond NREM sleep duration, and quantifying its SWA per minute sleep, NU1025 administration led to lower SWA compared with vehicle control (Figure 5N, O). Given that SWA is an established marker for sleep depth and sleep homeostasis (Franken et al., 2001), these experiments establish that inhibition of Parp1 activity in adult mice reduces the duration of NREM sleep and its intensity.

Discussion

Sleep benefits a variety of essential physiological mechanisms, from learning and memory to cellular maintenance in complex neuronal networks and individual neurons. The fundamental cellular functions of sleep may be conserved across evolution, as even animals with a simple nervous system sleep (Kanaya et al., 2020; Nath et al., 2017; Nelson and Raizen, 2013). Here, imaging of cellular and nuclear markers, coupled with behavioral monitoring of zebrafish, showed that neuronal DNA damage can be a driver for sleep that promotes DNA repair activity. There was a strong positive correlation ($R=0.76$) between levels of neuronal DNA damage and total sleep time (Figure 6A), suggesting that the amount of DNA damage can predict the total sleep time required for repair. Differences in the exposure to mutagenic factors and the susceptibility to DNA damage might therefore explain some intra- and inter-species variation in sleep quality and duration.

The results address the mechanisms by which accumulated DNA damage during wakefulness drives sleep, which promotes DNA repair (Figure 6B). Our causative experiments demonstrated that sleep increases the clustering of Rad52 and Ku80 repair proteins in neurons, which enable normalization of the levels of DNA damage. The DNA repair activity in neurons has mostly been studied in cell cultures and brain tissues (Barzilai et al., 2008; Thadathil et al., 2019). Mature neurons are non-dividing cells, and the HR pathway is presumed to be rarely used (Orii et al., 2006). Nevertheless, induction of DNA damage in neurons is followed by a transient increase in the expression of proteins involved in both HR and NHEJ and elevated DNA repair activity (Merlo et al., 2005). Our data support these findings and show that induction of various types of single- and double-strand breaks can increase the pressure for sleep-mediated repair (Figure 2, 3). We propose that the DDR systems are activated in real time upon generation of DNA damage during day and night, but that they are strongly upregulated during sleep, possibly because the cell resources can be dedicated to nuclear maintenance.

How does sleep promote efficient clustering of DDR proteins? Our results implicate chromosome dynamics since their inhibition abolished sleep-dependent DNA repair activity and resulted in accumulation of DNA damage. We suggest that the mechanism may involve movement and segregation of DNA fragments that provide accessibility to repair proteins, or alternatively there may be massive movements of chromosomes to repair centers in the nuclear periphery (Tsouroula et al., 2016). Notably, chromosome dynamics can regulate other key cellular processes that occur during sleep, such as the transcription of synaptic genes that regulate synaptic formation and elimination. Indeed, spatial movements and reorganization of large chromatin segments and regulation of promoter-enhancer interactions have been associated with memory formation (Marco et al., 2020). Thus, sleep regulates

DNA dynamics and repair, operations that promote chromatin stability that may modulate additional neuronal functions, including synaptic plasticity and memory consolidation.

Which molecules and pathways can sense the accumulation of nuclear DNA damage and promote sleep? PARP-1 is a DNA damage detector, which is recruited to DNA lesions with seconds (Liu et al., 2017) and subsequently initiates cascades of repair response (Pascal, 2018; Haince et al., 2008). In neurons of the zebrafish DP, Parp1 clustering in the nucleus increased during spontaneous wakefulness and post-SD, suggesting that Parp1 can monitor and signal the homeostatic pressure to sleep. Indeed, using genetic KD and inducible overexpression, we demonstrated that Parp1 is an essential regulator of sleep in zebrafish larvae. We further confirm that inhibiting Parp1 activity reduces sleep in mice. These results extend those of zebrafish larvae along three separate dimensions, by (i) establishing them in mammals and (ii) in adult animals, and (iii) by showing that Parp1 affects sleep depth, beyond its effects on sleep duration. Indeed, homeostatic sleep pressure is reflected both in the duration of NREM sleep, as well as in SWA levels representing its intensity (Borbély and Achermann, 1999).

Inhibition of Parp1 activity abolished DNA damage-induced sleep, chromosome dynamics, and repair, even under strong sleep pressure. In contrast to caffeine, which inhibits DNA repair while increasing neuronal activity and wakefulness (Selby and Sancar, 1990), the use of a Parp1 inhibitor inhibited repair activity and subsequently resulted in increased DNA damage without affecting neuronal activity. These results suggest that by detecting the accumulation of DNA damage, Parp1 pathway can signal the brain to promote sleep. Lack of this signal can mask the need to sleep even under increased DNA damage and homeostatic pressure. Intriguingly, clinical trials in cancer patients have concluded that fatigue is a prominent universal side effect for all FDA-approved PARP1 inhibitors (Janda et al., 2000; Knapp et al., 2012; LaFargue et al., 2019). Our findings suggest that these drugs mask the homeostatic signal to sleep and thereby cause sleep disturbance and chronic fatigue.

This study describes a molecular mechanism and a temporal cascade of nuclear processes that occur in single neurons during sleep and wakefulness (Figure 6B). This work in larval zebrafish provides a critical link between sleep studies in simple nervous systems of invertebrates and the complex mammalian brain. Since all animals with a nervous system studied so far sleep (Keene and Duboue, 2018), the cellular repair functions of sleep and the molecular regulators may be conserved. For example, p53 can regulate the sleep response in *C. elegans* (DeBardeleben et al., 2017), and the expression of various DDR markers are increased in sleep deprived humans (Cheung et al., 2019). Similarly, we found that the DDR initiator Parp1 regulates sleep homeostasis. PARP-1 has also been shown to modify components of the clock machinery (Asher et al., 2010) and is required for long-term memory (Cohen-Armon, 2004; Goldberg et al., 2009), suggesting a link between circadian and homeostatic processes and the regulation of sleep functions. Since this protein is already an attractive therapeutic target in cancer treatments (LaFargue et al., 2019), the drug effect on sleep and sleep disturbances can readily be examined in humans. Furthermore, our findings that sleep regulates the neuronal balance between DNA damage and repair and

consequently the health of the cell provide the basis for future work focusing on the causative link between sleep, aging, and neurodegenerative diseases.

Limitations of the study

Sleep is conserved across phylogeny, and experiments in additional model organisms could have broaden the conclusion. Indeed, our finding that Parp1 regulates sleep pressure in zebrafish larvae was validated in mice. These and future results can extend the proposed sleep mechanism to adult mammals and humans.

Sleep may regulate various DNA repair systems in a region-dependent manner. We focused on Rad52 and Ku80, which are key proteins in HR and NHEJ processes, respectively. Future experiments using additional repair markers and tools in various brain regions and cell types can further underline the molecular mechanism of sleep.

We studied neurons located in the DP because the activity of this region reduces during sleep and share commonalities with those of SWS and REM/PS in the mammalian cortex. Studying the mechanism regulating DNA damage and repair in additional sleep and wake regulatory circuits will be of interest.

STAR Methods

RESOURCE AVAILABILITY

Lead contact—Further information and requests for resources and reagents should be directed to the lead contact, Lior Appelbaum (lior.appelbaum@biu.ac.il).

Material availability—All plasmids and transgenic lines generated in this study are available from the Lead Contact.

Data and code availability

- The original raw data for imaging have been deposited in Mendeley Data (DOI:10.17632/xb39kmybzn.1).
- This paper does not report any original code.
- Any additional information required to reanalyze the data reported in this paper is available from the lead contact upon request.

EXPERIMENTAL MODEL AND SUBJECT DETAILS

Adult zebrafish (male and female) were raised and maintained in fully automated zebrafish housing systems (Aquazone, Israel; temperature 28 ± 0.5°C, pH 7.0, conductivity 500 μS) under 14 h light/10 h dark cycles, and fed twice a day. Embryos were produced by natural spawning and raised in egg-water containing methylene blue (0.3 ppm) in a light-controlled incubator at 28 ± 0.5°C, as previously described (Elbaz et al., 2012). The Tol2 system (Kawakami et al., 2004) was used to generate the transgenic lines *tg(uas:DsRed-Rad52), tg(uas:DsRed-TRF1)*, *tg(uas:Lap2β-EGFP)*, and *tg(dbh:Gal4)*. The transgenic lines *tg(HuC:Gal4), tg(HuC:GCaMP5)* and *tg(uas:ChR2-mCherry), and* both *tg(fli1:EGFP)* and

tg(sox10:EGFP) were kindly provided by Bettina Schmid (Ludwig Maximilian University of Munich, Germany), German Sumbre (Institute de Biologie- Ecole Normale Superieure, France), Herwig Baier (Max Planck Institute of Neurobiology, Germany), and Karina Yaniv (Weizmann Institute of Science, Israel), respectively.

Adult C57BL/6J male mice (~25g) were housed with their littermates. Throughout all housing and experiments, mice were under a 12 h light/ 12 h dark (LD) cycle with ambient temperature at 21–23C, and food/water available ad libitum. Experimental procedures, including animal handling, surgery, and sleep experiments, followed the National Institutes of Health's Guide for the care and use of laboratory animals. All animal protocols were reviewed and approved by the Bar-Ilan University and Tel Aviv University Bioethics Committee.

METHOD DETAILS

Behavioral assays.—Sleep was monitored as previously described (Elbaz et al., 2012). Briefly, larvae were individually placed in 48-well plates containing zebrafish housing system water. Larva-containing plates were placed in the Noldus DanioVision tracking system (Noldus Information Technology) with a light intensity of 70 LUX, and sleep was monitored under light and dark conditions (LD). In constant dark experiments (DD), the larvae were raised under 14/10 h LD cycle for 5 days and then placed in 48-well plates under constant darkness. Live video-tracking and analysis were conducted using the EthoVision XT 12 software (Noldus Information Technology). Data analyses of sleep time were performed according to the threshold parameters previously described (Elbaz et al., 2012).

SD was performed as previously described (Leung et al., 2019). Briefly, at ZT14, 6 dpf larvae were placed in 12.5 ml of system water in a 15 ml conical tube covered with aluminum foil. The conical tube was placed on a rotating platform that moves the air bubbles along the tube at a speed of 0.5 Hz, for 4 h under darkness (Figure S4A). The control group was also placed in a 15-ml conical tube under similar conditions except for the rotation. As a control experiment, the same protocol was applied during daytime wakefulness under light (Figure S4G).

In order to perform heat-shock inducible behavioral experiments, *pT2-hsp70:Gal4-* and *pT2-hsp70:Parp1*-injected larvae were raised in a 14/10 h LD cycle at 28°C. At 6 dpf, the larvae were placed in alternating wells in 48-well plate, and sleep was recorded during 1 h. Following 30 min of 37°C heat shock and recovery to 28°C, sleep was recorded for an additional 21 h.

Immunohistochemistry assays.—Larvae were fixed for 2–12 hours in 4% paraformaldehyde (PFA) in PBS at 4°C, and washed in PBST (PBS/0.1% Tween). The larvae were permeabilized with 20 μg/ml Proteinase K in PBST for 30 min at room temperature, followed by 6 × 5 min washes with PBST. The larvae were then blocked with 20% fetal bovine serum diluted in PBST for 1 hour at room temperature. Next, the larvae were incubated overnight at 4°C in blocking buffer with either of the following primary antibodies: rabbit anti-γH2AX (GTX127342, GeneTex), 1:250 dilution; rabbit anti-p44/42

MAPK (pERK, CST-4370S, Cell Signaling Technology), 1:500 dilution; or rabbit anti-Parp1 (Abcam, ab194586), 1:500 dilution. On the following day, larvae were washed in PBST and blocked for 1 hour. Anti- γH2AX, anti-MAPK, and anti-Parp1 were detected with a goat polyclonal secondary goat anti-rabbit IgG H&L (Alexa Fluor™ 488-A11008 or 594-A11012, Invitrogen) 1:200 dilution, in blocking buffer with DAPI/Antifade (250 ng/ml) counterstain (sc-3598, Santa Cruz Biotechnology) overnight at 4°C. The larvae were then washed in PBST and mounted for imaging.

In order to quantify the levels of DNA damage in specific cell types, we used the well-established phosphorylated histone γH2AX marker (Figure 1H, I, Figure S1C–E), which is activated in DNA damage sites and participates in the early cellular response to DNA breaks (Rogakou et al., 1998). Notably, in contrast to the findings in neurons, the number of γH2AX foci in myocytes, endothelial cells, and neuronal precursor cells did not change between day and night (Figure S1C–F).

Western blot.—For western blot, 6 dpf larvae were collected (pools of 35 larvae). The samples were lysed in 20mM Tris, pH 7.5, 150mM NaCl, 1mM EDTA, 1% Nonidet P-40, 0.5% sodium deoxycholate, 2 mM Na3VO4, 1 mM NaF, and 10 mM b-glycerophosphate. Lysates were incubated for 20 min on ice, and the supernatant was loaded after a 10 min spin at 13,000 rpm at 4°C. Protein concentration was determined by Bradford analysis. A total of 60 μg protein extract was loaded per lane on 10% SDS polyacrylamide gel. After electrophoresis, proteins were transferred to nitrocellulose membrane (BIO-RAD), and the membrane was blocked for 1 h in PBST with 5% skim milk. Next, the membrane was incubated in PBST with 5% skim milk containing the primary antibody against Parp1 antibody (Abcam, ab194586), diluted 1:1000, and against GAPDH antibody diluted 1:1000 (sc-47724, Santa Cruz Biotechnology) overnight at 4°C. After washing 3 × 5 min with PBST, the secondary antibody diluted 1:4000 [Peroxidase-conjugated AffiniPure Goat Anti-Rabbit IgG: 111-035-144 or Peroxidase-conjugated AffiniPure Goat Anti-Mouse IgG 115-035-062 (Jackson ImmunoResearch)] was incubated for 1 h at RT in PBST with 5% skim milk. Membrane development was performed following 3×5 min washing with PBST using EZ-ECL Kit according to the manufacturer's instructions (Biological Industries).

Comet assay.—The single cell gel electrophoresis (comet) assay was performed using the Comet Assay Kit (abcam ab238544) according to the manufacturer's protocol. In brief, 6 dpf larval brains were dissected and minced in a small amount of ice-cold PBS containing 20 mM EDTA. From each sample, 1×10^5 cells/ml were kept in ice-cold PBS. Cell samples were mixed with comet agarose in a 1/10 ratio (v/v) and immediately transferred onto the slide glasses covered with a comet agarose base layer. After incubating with pre-chilled lysis buffer, the slides were subjected to electrophoresis. Electrophoresis was performed in the Alkaline Electrophoresis Solution for the alkaline comet assay at 1 volt/cm for 15 min. After electrophoresis, the slides were incubated with Vista Green DNA dye.

The comet assay was used to detect DNA breaks in neurons extracted from 6 dpf larval brains during the day, night, subjective day, and post SD. Calculation of the comet tail moment (Olive et al., 1990) showed that the levels of DNA damage are increased during wakefulness (Figure S1A, B).

Transcription quantification of repair genes.—Relative mRNA quantification of *c-fos*, *rad52*, *ku80*, *apex1*, *ddb2, and parp1* was determined using qRT-PCR. Total RNA was extracted from 6–7 dpf larvae using the Direct-zol RNA MiniPrep kit (Zymo Research Corporation), according to the manufacturer's instructions. For each tested gene, a total of 5–14 biological samples were used. Each biological sample contained a pool of 10 larvae. mRNA (1 μg) was reverse-transcribed using qScript cDNA SuperMix (Quanta BioSciences). Relative transcript levels were determined by the CFX96™ Real-Time PCR (BIO-RAD). Duplicates of each cDNA sample were PCR-amplified using the PerfeCTa SYBR Green FastMix (Quanta BioSciences) and the following specific primers: *c-fos*: 5'-gctcaatcctacaacccgag-3' and 5'-cagccatcttgtttcgttcac-3'; *rad52*: 5'-cagaagttcagacaggagatgg-3' and 5'-gatctcgttgaaggatcgtcc-3'; *ku80*: 5'-atctccgtcagttcactttcc-3' and 5'-ctccattctcatccttctccatc-3'; *apex1*: 5'-agccaatatgaagatcacctcc-3' and 5'-ctttctcagcacacttggtttc-3'; *ddb2*: 5'-tgtggatgtgtctgttagcc-3' and 5'-tcacagcgagggttgaattc-3'; *parp1*: 5'-acacaagtctgctctacaacg-3' and 5'-acctctccagatctaaccgg-3'; and *rpl13*: 5'-agctcaagatggcaacacag-3' and 5'-aagttcttctcgtcctcc-3'. The relative quantification of each gene expression was normalized against *rpl13* mRNA expression levels and subjected to the ΔΔCT method (Elbaz et al., 2012).

In order to select and establish repair markers, we initially screened the expression levels of genes involved in various DDR pathways during the day and night. Quantitative reverse transcription PCR (qRT-PCR) was used to assess the expression of *rad52, ku80, apex1,* and *ddb2*, which are key DNA repair proteins in the HR, NHEJ, BER, and NER pathways, respectively. Under normal day/night cycle, the expression of all transcripts was rhythmic and increased during the day (ZT4, Figure S4C–F). However, SD (Figure S4A, B) increased the expression of only *rad52* and *ku80* mRNA (ZT18) compared to the night control groups. These results indicate that the rhythmic transcription of the DDR genes is predominantly controlled by the light/dark cycle, although homeostatic sleep pressure can also regulate the transcription of *rad52* and *ku80*. Although high transcription levels of *rad52* and *ku80* were observed in whole larvae during daytime wakefulness and following SD (Figure S4C, D), this reflects the expression of mRNA, and not necessarily the levels of protein. Furthermore, the lag time between the expression of mRNA, and protein translation and activity can be a matter of hours. For example, the transcription of synaptic genes is primarily regulated by the circadian clock, while the translation of the encoded protein is driven by sleep (Noya et al., 2019). To overcome this issue, in repair experiments, we monitored the activity and clustering of DDR proteins.

DNA constructs.—*pT2-uas:DsRed-Rad52* was generated by amplifying the coding sequences of *rad52* (NM_001024451.1) and *DsRed* using the following primers: *rad52*: 5'-aagACCGGTatggattatagcagcgggagg-3' and 5'-aggCTCGAGtcacgtgtccaatcttcgtttct-3'; *DsRed*: 5'-accGAATTCaccatggctccaaagaagaagcgtaaggtaatgaagcttgcctcctccga-3' and 5'-catACCGGTggttagtggtggtggtggtgg-3' (*nls* sequence is underlined). Triple ligation of *EcoRI*/*XhoI*-digested *pT2-uas:MCS* vector (kindly provided by Didier Stainier, Max Planck Institute, Germany), *EcoRI*/*AgeI*-digested *DsRed*, and *AgeI*/*XhoI*-digested *rad52* was performed.

pT2-uas:Ku80-EGFP was generated by amplifying the coding sequences of *ku80/xrcc5* (NM_001017360.2) and *egfp* using the following primers: *ku80*: 5'-attGAATTCatggcgcgagcagcgaagt-3' and 5'- cccGAATTCcatcatgtccagcagatca-3'; *egfp*: 5'-attGAATTCatggtgagcaagggcgagga-3' and 5'- ggCTCGAGatatcttacttgtacagctcgt -3'. Triple ligation of *EcoRI*/*XhoI*-digested *pT2-uas:MCS* vector, *EcoRI*-digested *ku80*, and *EcoRI*/*XhoI*-digested *egfp* was performed.

Mutation in *rad52* (*rad52*^{R49A}) and *ku80 (ku80*$^{D721A/D722A}$) genes were introduced using PCR deletion and substitution of single nucleotides in the *pT2-uas:DsRed-Rad52* and *pT2-uas:Ku80-EGFP* vectors, respectively, using the following primer: *rad52*^{R49A}: 5'-gcacaggctggaggaggacaaaaggt-3' and 5'- ggtgctgatgtattcaggtccgag-3'; *ku80*$^{D721A/D722A}$: 5'-gccactgctggacatgatgt-3' and 5'-tgccacatctccagtgtcgt-3' (the sites of mutations are underlined). Mutation in *lap2β* gene (*lap2β*^{LEMdel}) was introduced using PCR deletion of 135 nucleotides (amino acids D92-G136) in the *pT2-uas:Lap2β-EGFP* vector, using the following primer: 5'-ctcctgtagctgtggctcttc-3' and 5'-gtcaggacgaactttgtcgg-3'.

pT2-hsp70:Parp1 was generated by amplifying the coding sequences of *Parp1* (NM_001044942.1) using the following primers: 5'-aagagaGGATCCatggccgactca caggacgacaagctgtac-3' and 5'-aagagaATCGATtcaccacagagacgtctgatagttgaagcgga-3'. Ligation of *BamHI*/*ClaI*-digested *pT2-hsp70:Gal4* vector (kindly provided by Karina Yaniv, Weizmann Institute of Science, Israel) and *BamHI*/*ClaI*-digested *Parp1* was performed.

pT2-dbh:Gal4 was generated by amplifying ~1.1 kbp fragment, located upstream to the zebrafish *dbh* gene, using the following primers 5′-aatGGGCCCacttgaaccagcgaccttct-3′ and 5′- ccgACCGGTggtttgaaggcctttctaagttttt-3′, as previously described (Liu et al., 2015). The PCR product was digested with *ApaI* and *AgeI* restriction enzymes and cloned into *ApaI*- and *AgeI*-digested *pT2-mbp:Gal4* vector (Zada et al., 2019), replacing the *mbp* promoter.

Establishment of DNA repair reporter proteins—The DsRed-Rad52 and Ku80-EGFP markers were expressed in larvae. Under naïve daytime conditions, ubiquitous nuclear expression was observed in most neurons, while DsRed-Rad52 clusters were observed in only a few neurons (Figure 3C, D, S3K). In order to validate that DsRed-Rad52 proteins are recruited into DNA damage sites, *tg(HuC:Gal4/uas:DsRed-Rad52)* larvae were analyzed by immunohistochemistry using the γH2AX antibody. The elav/HuC promoter and protein is an established neuronal marker in zebrafish. As expected, punctate structures of co-localized γH2AX and DsRed-Rad52 were observed in the nucleus (Figure S4K). To further validate that the DsRed-Rad52 clusters are localized in DNA binding sites, we introduced a point mutation that converted the conserved 49th amino acid arginine into alanine (A, DsRed-Rad52^{R49A}). Notably, a similar mutation (R55A) in human cells abolished the ssDNA-binding function of RAD52 (Kagawa et al., 2002). Transient expression of DsRed-Rad52^{R49A} resulted in the formation of large nuclear protein aggregates that did not co-localize with γH2AX (Figure S4L). In order to visualize the expression pattern of Ku80-EGFP, the *pT2-uas:Ku80-EGFP* construct was injected into *tg(HuC:Gal4)* larvae. While ubiquitous nuclear Ku80-EGFP expression was observed in most neurons, a few neurons exhibited punctate Ku80-EGFP clusters (Figure S4M). Imaging of the γH2AX and Ku80-EGFP clusters showed that the proteins do not co-localize (Figure S4M), which

is in accordance with the results in a human cell line (Britton et al., 2013). In order to validate that the Ku80-EGFP clusters bind to DNA sites, we introduced point mutations in the 721–722 residues ($Ku80^{D721A/D722A}$) since similar mutations in human KU80 impaired the recruitment of KU80 to DNA damage sites (Falck et al., 2005). Transient expression of $Ku80^{D721A/D722A}$-EGFP, resulted in large protein aggregates in the nucleus (Figure S4N). These assays show that DsRed-Rad52 and Ku80-EGFP foci are dynamically bound to DNA sites and can be used as reporters for the activity of the repair systems.

Cas9/CRISPR-based KD and microinjection assays.—In order to KD *parp1*, we used the modified CRISPR/Cas9 protocol as previously described (Kroll et al., 2021). Three *parp1* specific sgRNAs were designed and synthesized by IDT (Alt-R CRISPR-Cas9 System): sgRNA1, ggccgcagttcagtctcctt; sgRNA2, cagcttggtctaatcgatcg; and sgRNA3, gagcatgaagaaagccatgg. The sgRNA's were diluted in IDTE buffer to 100 μM stock solution, according to the manufacturer's protocol. The control scrambled sgRNA caatcgagacattccagtag was cloned into the DR274 plasmid (Addgene) and synthesized using the T7 High Yield RNA Synthesis Kit (NEB). Pre-assembled RNPs composed of Cas9 protein and sgRNA are highly effective in zebrafish. Therefore, RNPs generated before the microinjection by mixing 4 μg/μl of Alt-R® S.p. Cas9 Nuclease V3 (IDT) and 600 ng/μl of each sgRNA, incubation at 37°C for 5 min, and chilled in ice-cold water. Injection of control RNPs and *parp1* RNPs resulted in 13.8% and 29.6% mortality, respectively. Among the surviving larvae, 3.7% (control) and 45.9% (*parp1*) displayed developmental abnormalities.

The expression of the RNPs and the DNA constructs *pT2-uas:DsRed-Rad52*^{R49A}, *pT2-uas:Ku80-EGFP*, *pT2-uas:ku80*$^{D721A/D722A}$*-EGFP*, *pT2-hsp70:Gal4,* and *pT2-hsp70:Parp1*, at a concentration of 30 ng/μl, were performed by microinjection of approximately 2 nl of each solution into one-cell-stage embryos, using a micromanipulator and PV830 Pneumatic PicoPump (World Precision Instruments).

Imaging.—All imaging experiments were conducted on 5–7 dpf larvae. Larvae were mounted in low-melting-point agarose 1.5%. Imaging was performed using a Zeiss LSM710 upright confocal/two-photon microscope with either ×20, 1.0 NA or ×63, 1.0 NA objectives. The DsRed-Rad52, DsRed-TRF1, and Alexa Fluor™ 594 were imaged using DPSS 561 nm, the Ku80-EGFP, Lap2β-EGFP, and Alexa Fluor™ 488 were imaged using Argon 488 nm. The DAPI was imaged using Diode 405nm.

In chromosome dynamics imaging, we used the following parameters: image resolution of 256 × 256, 30 planes, speed of 242.04 ms per plane. One plane size was typically 16.9 × 16.9 × 1.3 μm, with intervals of 0.3 μm between planes in all Z stacks.

In *HuC*-driven GCaMP5 imaging, 6 dpf *tg(HuC:GCaMP5)* larvae were mounted, and the GCaMP5 signal was monitored using a Mai-Tai 2-photon laser, tuned to 920 nm, with a ×20 1.0 NA objective. Scanning was performed at a single plane for 20 min at 4.13 Hz.

Optogenetic experiments.—The *tg(uas:ChR2-mCherry)* and *tg(HuC:Gal4)* lines were crossed, and *mCherry*-positive and -negative control embryos were raised under 14 h light/10 h dark cycles in the same Petri dish. At 6 dpf, *mCherry*-positive and -negative larvae

were placed in alternating wells in a 48 well plate, and sleep was monitored over 2 h. All larvae were then stimulated for 10 min with blue light (480 nm, light on: 1 Hz/30 ss, light off: 30 s), and sleep monitoring was resumed. In the immunohistochemistry experiments, the same protocol was applied, and *mCherry*-positive and -negative larvae were fixed at various time points post stimuli. In the comet assays, *mCherry*-positive and -negative larvae were sampled 30 minutes following the stimuli.

Pharmacological and UV radiation experiments.—During the daytime, 6 dpf larvae were treated for 30 min with either 5% DMSO or 10 mM PTZ (Sigma-Aldrich) dissolved in DMSO and diluted in the zebrafish system water. Sleep time and DNA damage and the clustering of repair proteins were monitored immediately, and 1, 2, and 3 h following the treatment.

In addition, 6 dpf larvae were treated for 2 h with either 0.0001% DMSO or 10 μM ETO (Sigma-Aldrich) diluted in zebrafish system water. Chromosome dynamics, pERK levels, and clustering of repair proteins were monitored before, during, and following the treatment.

In Parp1 inhibitor experiments, 5–6 dpf larvae were treated with either 1% DMSO, 50 μM, or 100 μM NU1025 (Sigma-Aldrich) dissolved in DMSO and diluted in zebrafish water. Sleep time and DNA damage and *c-fos* transcript levels were monitored during and following the treatment.

In UV radiation experiments, 6 dpf larvae were exposed for 2 min to 5–10 mW/cm^2 UV radiation (302 nm). The control groups were exposed to purple light for 2 min. Sleep time, pERK levels, DNA damage, chromosome dynamics, and clustering of repair proteins were monitored before and following the exposure.

Data analysis in zebrafish experiments.—The number of γH2AX, Parp1, Rad52, and Ku80 foci per nuclei were quantified using the “Cell Counter” plugin in ImageJ (NIH). The images of Rad52 and Ku80 markers were subjected to “Subtract Background” with a rolling ball radius of 30 pixels. In comet assay analysis, four pictures were randomly taken from each group, and the tail moment was calculated using the OpenComet plugin in ImageJ (NIH). In experiments considering pERK expression, approximately 40 DP DAPI-stained neurons per larvae were selected as regions of interest (ROI, ImageJ). The mean gray value was extracted and normalized to the control group in each experiment. As previously described (Bronshtein et al., 2016; Zada et al., 2019), chromosome dynamics were analyzed using Imaris software (Oxford Instruments) for punctum coordinates and correction of nuclear drift and rotation. Custom-made MATLAB software (Mathworks) was used to quantify the volume of motion of each punctum in single nuclei. In calcium imaging analysis, time-lapse movies were registered to remove drifts using the template matching plugin in ImageJ. ROI selection, ΔF/F, and raster plots were prepared using the custom-made MATLAB (Mathworks) programs FindROI and ProcessCalciumData (Romano et al., 2017).

Mouse surgery.—Surgical procedures for EEG/EMG electrode implantation follow our previous work (Atlan et al., 2021; Rodriguez et al., 2016). Perioperative analgesia

and antibiotic prophylaxis follow procedures as in (Sela et al., 2020). Briefly, mice were anesthetized using isoflurane (4% induction, 1%–2% maintenance) and placed in a stereotactic frame (David Kopf Instruments). The head was shaved, and Viscotear gel was applied to protect the eyes. After exposing and cleaning the skull, frontal and parietal screws (1 mm in diameter) were placed over the right hemisphere for EEG recording. Two additional screws were placed above the cerebellum as reference and ground. Two single-stranded stainless-steel wires were inserted to either side of neck muscles to measure EMG. EEG and EMG wires were soldered onto a custom-made headstage connector. Dental cement was used to cover all screws and EEG/EMG wires.

Electrophysiology in mice.—EEG and EMG were digitally sampled at 1017Hz (PZ2 amplifier, Tucker-Davis Technologies (TDT)), and filtered online: both signals were notch-filtered at 50Hz and harmonics to ensure removal of any residual line noise (RZ2, TDT). Bipolar referencing was applied to EMG signals (EMG1 – EMG2). Next, EEG and EMG were band-pass filtered at 0.5–200Hz and 10–100Hz, respectively. Simultaneous video data were captured by a USB webcam synchronized with electrophysiology data. Offline, EEG and EMG were resampled to 1000Hz (MATLAB, Mathworks) for subsequent analysis.

At least one week was allowed for surgical recovery and habituation before any experiments. Three days after surgery, mice were moved individually to a new Perspex home cage placed within a sound-attenuation chamber (40dB attenuation, H.N.A). At least four additional days were given for habituation to the new environment and to daily i.p. saline injections (250 μl) at light onset, as well as to being tethered to recording cables. We then performed seven experimental recording days as follows. In days number 2, 4 and 6, mice received an i.p. injection (250 μl) at light onset of either (1) vehicle (40% polyethylene glycol-200 [PEG-200, Sigma-Aldrich] in saline), (2) 5 mg/kg, or (3) 10 mg/kg NU1025 (Sigma-Aldrich) dissolved in 40% PEG-200 in saline. The order of the three experimental conditions was randomly assigned in each animal. In the other four ‘baseline’ days we injected 250 μl of saline. Due to technical issues, data were not available in 4 out of 63 sessions (7 sessions × 9 mice). In two subjects, vehicle data were replaced with saline (we could not observe differences between saline and vehicle conditions, see Figure S6E–G). In two subjects, only one dose of NU1025 was available.

Sleep scoring in mice.—Sleep scoring (Figure S6A–D) was performed blindly to experimental conditions via detailed combined manual examination of frontal and parietal EEG, EMG, and video, using custom MATLAB software, which enabled precise marking of state transitions as in (Sela et al., 2020). Data were divided to three vigilance states (1) wakefulness: low-voltage high-frequency EEG, and high tonic EMG, with intermittent bouts of phasic EMG and behavioral activity confirmed with video (e.g., eating, grooming, locomotion); (2) NREM sleep: high-amplitude SWA and low tonic EMG; (3) REM sleep: high-frequency wake-like frontal EEG co-occurring with theta activity in parietal EEG and flat EMG. In addition, 4.47 ± 6.5% of data intervals were marked as artifacts and excluded from subsequent spectral data analysis of SWA. Joint distributions of EMG levels and EEG high-/low-frequency power ratio (Figure S6C) were calculated in 4s epochs. EEG power spectrum in each vigilance state was calculated across entire 8 h datasets in 4s

temporal windows using Matlab's 'pwelch' function. Power ratio was defined as power > 25 Hz divided by power < 5 Hz in the frontal EEG. A within-subject design compared the effects of intraperitoneal (i.p.) injections of the Parp1 inhibitor NU1025 vs. vehicle (in a counterbalanced order) on sleep/wake dynamics. Offline sleep scoring was performed in a manner blind to experimental conditions (Figure S6). In line with the literature (Soltani et al., 2019), during the first 8 h following 'lights on' in baseline sessions (saline injection), mice spent 28%, 58%, and 6% of their time in wakefulness, non-rapid eye movement (NREM) sleep, and rapid eye movement (REM) sleep, respectively (Figure S6A–D). EEG power spectra exhibited characteristic profiles including increased slow wave activity (SWA) in NREM sleep, and higher theta/high-frequency activity in wakefulness and REM sleep (Figure S6B, C). Notably, sleep patterns were comparable in vehicle-injection and saline-injection sessions, and we could not detect significant differences in the amount of NREM sleep or in NREM SWA levels (Figure S6E–G). After the initial 45 min post-injection, the prevalence of NREM sleep was maximal (~80% of time), as expected shortly after light onset.

Data analysis in mouse experiments.—In each subject separately, we averaged the results in the two NU1025 conditions (since we could not observe any dose-dependent differences), and compared this average to the vehicle condition. Dynamics of percent time in NREM sleep (Figure 5L & Figure S6E) were calculated, for each session separately, in the first 8 h after light onset in 15 min bins. Quantification and statistics (Figure 5M & Figure S6F) focused on the 0.75–1.5 h time interval following 'lights-on' and injection.

SWA (Figure 5N, O, Figure S6G) was calculated as the average power spectral density below 4Hz ('pwelch' function in Matlab) using 4s segments. SWA was normalized (i) per minute of NREM sleep, to go beyond sleep duration, and (ii) expressed as percent of that in the baseline (saline) session performed on a different day, separately in each mouse and separately for vehicle and NU1025 conditions. Quantification and statistics (Figure 5O) was performed in all subjects with a minimum of 3 min of NREM sleep in the 0.75–1.5 h time interval.

Quantification and statistical analysis.—All imaging experiments were performed independently on at least four batches. Differences between two categorical groups on continuous variables were determined by two-way ANOVA followed by post-hoc Tukey's test using MATLAB (Mathworks). Differences between more than two groups were determined using one-way ANOVA followed by post-hoc Tukey's test using MATLAB (Mathworks). Differences between the two groups were determined by a two-tailed *t*-test: two samples assuming unequal variance using Analysis ToolPac in Excel (Microsoft). Differences between two paired groups were determined by one-tailed sign-rank test using MATLAB (Mathworks). The correlation between sleep time and γH2AX foci number was determined by Pearson correlation coefficient using the social science statistics calculator.

Supplementary Material

Refer to Web version on PubMed Central for supplementary material.

Acknowledgments

The Appelbaum lab is supported by the Israel Science Foundation (ISF, grant no. 961/19), the United States—Israel Binational Science Foundation (BSF, grant no. 2017105), National Science Foundation (NSF) - BSF joint funding EDGE program (NSF-BSF grant no. 2019604), and the National Institute of Health (NIH, R01 MH116470). Research in the Nir lab is supported by ISF grants 1326/15 and 51/11 (I-CORE Cognitive Sciences), the Adelis Foundation, the European Research Council (ERC-2019-CoG 864353), and by an Azrieli Foundation fellowship award (YS). We thank Ann Avron and Yael Laure for assistance in editing the manuscript and Dr. Noa Alon for assistance in designing the schematic illustrations; Dr. Alona Zilberberg, Dr. Sally Shpunigin, and the members of the Appelbaum lab for technical assistance; Dr. Noa Regev, Itai Caspit, Arielle Lavi, and Talia Engel for assistance with mouse experiments and sleep scoring.

References

Allada R, and Siegel JM (2008). Unearthing the phylogenetic roots of sleep. Curr. Biol. CB 18, R670–R679. [PubMed: 18682212]

Allada R, Cirelli C, and Sehgal A (2017). Molecular Mechanisms of Sleep Homeostasis in Flies and Mammals. Cold Spring Harb. Perspect. Biol 9.

Asher G, Reinke H, Altmeyer M, Gutierrez-Arcelus M, Hottiger MO, and Schibler U (2010). Poly(ADP-ribose) polymerase 1 participates in the phase entrainment of circadian clocks to feeding. Cell 142, 943–953. [PubMed: 20832105]

Atlan G, Matosevich N, Peretz-Rivlin N, Yvgi I, Chen E, Kleinman T, Bleistein N, Sheinbach E, Groysman M, Nir Y, et al. (2021). Claustral Projections to Anterior Cingulate Cortex Modulate Engagement with the External World (Neuroscience)

Baraban SC, Taylor MR, Castro PA, and Baier H (2005). Pentylenetetrazole induced changes in zebrafish behavior, neural activity and c-fos expression. Neuroscience 131, 759–768. [PubMed: 15730879]

Barzilai A, Biton S, and Shiloh Y (2008). The role of the DNA damage response in neuronal development, organization and maintenance. DNA Repair 7, 1010–1027. [PubMed: 18458000]

Beck C, Robert I, Reina-San-Martin B, Schreiber V, and Dantzer F (2014). Poly(ADP-ribose) polymerases in double-strand break repair: focus on PARP1, PARP2 and PARP3. Exp. Cell Res 329, 18–25. [PubMed: 25017100]

Bellesi M, Bushey D, Chini M, Tononi G, and Cirelli C (2016). Contribution of sleep to the repair of neuronal DNA double-strand breaks: evidence from flies and mice. Sci. Rep 6, 36804. [PubMed: 27830758]

Borbély AA (1982). A two process model of sleep regulation. Hum. Neurobiol 1, 195–204. [PubMed: 7185792]

Borbély AA, and Achermann P (1999). Sleep homeostasis and models of sleep regulation. J. Biol. Rhythms 14, 557–568. [PubMed: 10643753]

Bowman KJ, Newell DR, Calvert AH, and Curtin NJ (2001). Differential effects of the poly (ADP-ribose) polymerase (PARP) inhibitor NU1025 on topoisomerase I and II inhibitor cytotoxicity in L1210 cells in vitro. Br. J. Cancer 84, 106–112. [PubMed: 11139322]

Britton S, Coates J, and Jackson SP (2013). A new method for high-resolution imaging of Ku foci to decipher mechanisms of DNA double-strand break repair. J. Cell Biol 202, 579–595. [PubMed: 23897892]

Bronshtein I, Kanter I, Kepten E, Lindner M, Berezin S, Shav-Tal Y, and Garini Y (2016). Exploring chromatin organization mechanisms through its dynamic properties. Nucl. Austin Tex 7, 27–33.

Caridi CP, D'Agostino C, Ryu T, Zapotoczny G, Delabaere L, Li X, Khodaverdian VY, Amaral N, Lin E, Rau AR, et al. (2018). Nuclear F-actin and myosins drive relocalization of heterochromatic breaks. Nature 559, 54–60. [PubMed: 29925946]

Carroll JE, Cole SW, Seeman TE, Breen EC, Witarama T, Arevalo JMG, Ma J, and Irwin MR (2016). Partial sleep deprivation activates the DNA damage response (DDR) and the senescence-associated secretory phenotype (SASP) in aged adult humans. Brain. Behav. Immun 51, 223–229. [PubMed: 26336034]

Cayuela ML, Claes KBM, Ferreira MG, Henriques CM, van Eeden F, Varga M, Vierstraete J, and Mione MC (2018). The Zebrafish as an Emerging Model to Study DNA Damage in Aging, Cancer and Other Diseases. Front. Cell Dev. Biol 6, 178. [PubMed: 30687705]

Cheung V, Yuen VM, Wong GTC, and Choi SW (2019). The effect of sleep deprivation and disruption on DNA damage and health of doctors. Anaesthesia 74, 434–440. [PubMed: 30675716]

Cohen-Armon M (2004). Long-Term Memory Requires PolyADP-ribosylation. Science 304, 1820–1822. [PubMed: 15205535]

DeBardeleben HK, Lopes LE, Nessel MP, and Raizen DM (2017). Stress-Induced Sleep After Exposure to Ultraviolet Light Is Promoted by p53 in Caenorhabditis elegans. Genetics 207, 571–582. [PubMed: 28754659]

Dechat T, Vlcek S, and Foisner R (2000). Review: lamina-associated polypeptide 2 isoforms and related proteins in cell cycle-dependent nuclear structure dynamics. J. Struct. Biol 129, 335–345. [PubMed: 10806084]

Eban-Rothschild A, Appelbaum L, and de Lecea L (2017). Neuronal Mechanisms for Sleep/Wake Regulation and Modulatory Drive. Neuropsychopharmacol. Off. Publ. Am. Coll. Neuropsychopharmacol

Elbaz I, Yelin-Bekerman L, Nicenboim J, Vatine G, and Appelbaum L (2012). Genetic ablation of hypocretin neurons alters behavioral state transitions in zebrafish. J. Neurosci. Off. J. Soc. Neurosci 32, 12961–12972.

Falck J, Coates J, and Jackson SP (2005). Conserved modes of recruitment of ATM, ATR and DNA-PKcs to sites of DNA damage. Nature 434, 605–611. [PubMed: 15758953]

Franken P, Chollet D, and Tafti M (2001). The Homeostatic Regulation of Sleep Need Is under Genetic Control. J. Neurosci 21, 2610–2621. [PubMed: 11306614]

Gerlai R (2020). Evolutionary conservation, translational relevance and cognitive function: The future of zebrafish in behavioral neuroscience. Neurosci. Biobehav. Rev 116, 426–435. [PubMed: 32681940]

Goldberg S, Visochek L, Giladi E, Gozes I, and Cohen-Armon M (2009). PolyADP-ribosylation is required for long-term memory formation in mammals. J. Neurochem 111, 72–79. [PubMed: 19645746]

Gravett N, Bhagwandin A, Sutcliffe R, Landen K, Chase MJ, Lyamin OI, Siegel JM, and Manger PR (2017). Inactivity/sleep in two wild free-roaming African elephant matriarchs - Does large body size make elephants the shortest mammalian sleepers? PloS One 12, e0171903. [PubMed: 28249035]

Haince J-F, McDonald D, Rodrigue A, Déry U, Masson J-Y, Hendzel MJ, and Poirier GG (2008). PARP1-dependent kinetics of recruitment of MRE11 and NBS1 proteins to multiple DNA damage sites. J. Biol. Chem 283, 1197–1208. [PubMed: 18025084]

Harper JW, and Elledge SJ (2007). The DNA damage response: ten years after. Mol. Cell 28, 739–745. [PubMed: 18082599]

Hayat H, Regev N, Matosevich N, Sales A, Paredes-Rodriguez E, Krom AJ, Bergman L, Li Y, Lavigne M, Kremer EJ, et al. (2020). Locus coeruleus norepinephrine activity mediates sensory-evoked awakenings from sleep. Sci. Adv 6, eaaz4232. [PubMed: 32285002]

Helmbrecht TO, Dal Maschio M, Donovan JC, Koutsouli S, and Baier H (2018). Topography of a Visuomotor Transformation. Neuron 100, 1429–1445.e4. [PubMed: 30392799]

Hill AJ, Mansfield R, Lopez JMNG, Raizen DM, and Van Buskirk C (2014). Cellular stress induces a protective sleep-like state in C. elegans. Curr. Biol. CB 24, 2399–2405. [PubMed: 25264259]

Hirshkowitz M, Whiton K, Albert SM, Alessi C, Bruni O, DonCarlos L, Hazen N, Herman J, Adams Hillard PJ, Katz ES, et al. (2015). National Sleep Foundation's updated sleep duration recommendations: final report. Sleep Health 1, 233–243. [PubMed: 29073398]

Jackson SP, and Bartek J (2009). The DNA-damage response in human biology and disease. Nature 461, 1071–1078. [PubMed: 19847258]

Janda M, Gerstner N, Obermair A, Fuerst A, Wachter S, Dieckmann K, and Pötter R (2000). Quality of life changes during conformal radiation therapy for prostate carcinoma. Cancer 89, 1322–1328. [PubMed: 11002229]

Joiner WJ (2016). Unraveling the Evolutionary Determinants of Sleep. Curr. Biol. CB 26, R1073–R1087. [PubMed: 27780049]

Kagawa W, Kurumizaka H, Ishitani R, Fukai S, Nureki O, Shibata T, and Yokoyama S (2002). Crystal structure of the homologous-pairing domain from the human Rad52 recombinase in the undecameric form. Mol. Cell 10, 359–371. [PubMed: 12191481]

Kanaya HJ, Park S, Kim J-H, Kusumi J, Krenenou S, Sawatari E, Sato A, Lee J, Bang H, Kobayakawa Y, et al. (2020). A sleep-like state in Hydra unravels conserved sleep mechanisms during the evolutionary development of the central nervous system. Sci. Adv 6.

Karanam K, Kafri R, Loewer A, and Lahav G (2012). Quantitative live cell imaging reveals a gradual shift between DNA repair mechanisms and a maximal use of HR in mid S phase. Mol. Cell 47, 320–329. [PubMed: 22841003]

Kawakami K, Takeda H, Kawakami N, Kobayashi M, Matsuda N, and Mishina M (2004). A transposon-mediated gene trap approach identifies developmentally regulated genes in zebrafish. Dev. Cell 7, 133–144. [PubMed: 15239961]

Keene AC, and Duboue ER (2018). The origins and evolution of sleep. J. Exp. Biol 221.

Knapp K, Cooper B, Koetters T, Cataldo J, Dhruva A, Paul SM, West C, Aouizerat BE, and Miaskowski C (2012). Trajectories and predictors of symptom occurrence, severity, and distress in prostate cancer patients undergoing radiation therapy. J. Pain Symptom Manage 44, 486–507. [PubMed: 22771128]

Kroll F, Powell GT, Ghosh M, Gestri G, Antinucci P, Hearn TJ, Tunbak H, Lim S, Dennis HW, Fernandez JM, et al. (2021). A simple and effective F0 knockout method for rapid screening of behaviour and other complex phenotypes. ELife 10, e59683. [PubMed: 33416493]

LaFargue CJ, Dal Molin GZ, Sood AK, and Coleman RL (2019). Exploring and comparing adverse events between PARP inhibitors. Lancet Oncol 20, e15–e28. [PubMed: 30614472]

Langelier M-F, and Pascal JM (2013). PARP-1 mechanism for coupling DNA damage detection to poly(ADP-ribose) synthesis. Curr. Opin. Struct. Biol 23, 134–143. [PubMed: 23333033]

Lawson ND, and Weinstein BM (2002). In vivo imaging of embryonic vascular development using transgenic zebrafish. Dev. Biol 248, 307–318. [PubMed: 12167406]

Lenz O, Xiong J, Nelson MD, Raizen DM, and Williams JA (2015). FMRFamide signaling promotes stress-induced sleep in Drosophila. Brain. Behav. Immun 47, 141–148. [PubMed: 25668617]

Leung LC, Wang GX, and Mourrain P (2013). Imaging zebrafish neural circuitry from whole brain to synapse. Front. Neural Circuits 7, 76. [PubMed: 23630470]

Leung LC, Wang GX, Madelaine R, Skariah G, Kawakami K, Deisseroth K, Urban AE, and Mourrain P (2019). Neural signatures of sleep in zebrafish. Nature 571, 198–204. [PubMed: 31292557]

Liu C, Vyas A, Kassab MA, Singh AK, and Yu X (2017). The role of poly ADP-ribosylation in the first wave of DNA damage response. Nucleic Acids Res 45, 8129–8141. [PubMed: 28854736]

Liu J, Merkle FT, Gandhi AV, Gagnon JA, Woods IG, Chiu CN, Shimogori T, Schier AF, and Prober DA (2015). Evolutionarily conserved regulation of hypocretin neuron specification by Lhx9. Development

Lockley SW, Evans EE, Scheer FAJL, Brainard GC, Czeisler CA, and Aeschbach D (2006). Short-wavelength sensitivity for the direct effects of light on alertness, vigilance, and the waking electroencephalogram in humans. Sleep 29, 161–168. [PubMed: 16494083]

Mackiewicz M, Shockley KR, Romer MA, Galante RJ, Zimmerman JE, Naidoo N, Baldwin DA, Jensen ST, Churchill GA, and Pack AI (2007). Macromolecule biosynthesis: a key function of sleep. Physiol. Genomics 31, 441–457. [PubMed: 17698924]

Madabhushi R, Gao F, Pfenning AR, Pan L, Yamakawa S, Seo J, Rueda R, Phan TX, Yamakawa H, Pao P-C, et al. (2015). Activity-Induced DNA Breaks Govern the Expression of Neuronal Early-Response Genes. Cell 161, 1592–1605. [PubMed: 26052046]

Marco A, Meharena HS, Dileep V, Raju RM, Davila-Velderrain J, Zhang AL, Adaikkan C, Young JZ, Gao F, Kellis M, et al. (2020). Mapping the epigenomic and transcriptomic interplay during memory formation and recall in the hippocampal engram ensemble. Nat. Neurosci 23, 1606–1617. [PubMed: 33020654]

Merlo D, Di Stasi AMM, Bonini P, Mollinari C, Cardinale A, Cozzolino F, Wisden W, and Garaci E (2005). DNA repair in post-mitotic neurons: a gene-trapping strategy. Cell Death Differ 12, 307–309. [PubMed: 15665815]

Nath RD, Bedbrook CN, Abrams MJ, Basinger T, Bois JS, Prober DA, Sternberg PW, Gradinaru V, and Goentoro L (2017). The Jellyfish Cassiopea Exhibits a Sleep-like State. Curr. Biol. CB

Nelson MD, and Raizen DM (2013). A sleep state during C. elegans development. Curr. Opin. Neurobiol 23, 824–830. [PubMed: 23562486]

Noya SB, Colameo D, Brüning F, Spinnler A, Mircsof D, Opitz L, Mann M, Tyagarajan SK, Robles MS, and Brown SA (2019). The forebrain synaptic transcriptome is organized by clocks but its proteome is driven by sleep. Science 366.

Olive PL, Banáth JP, and Durand RE (1990). Heterogeneity in radiation-induced DNA damage and repair in tumor and normal cells measured using the “comet” assay. Radiat. Res 122, 86–94. [PubMed: 2320728]

Orii KE, Lee Y, Kondo N, and McKinnon PJ (2006). Selective utilization of nonhomologous end-joining and homologous recombination DNA repair pathways during nervous system development. Proc. Natl. Acad. Sci. U. S. A 103, 10017–10022. [PubMed: 16777961]

Pascal JM (2018). The comings and goings of PARP-1 in response to DNA damage. DNA Repair 71, 177–182. [PubMed: 30177435]

Pei D-S, and Strauss PR (2013). Zebrafish as a model system to study DNA damage and repair. Mutat. Res. Mol. Mech. Mutagen 743–744, 151–159.

Plucińska G, Paquet D, Hruscha A, Godinho L, Haass C, Schmid B, and Misgeld T (2012). In vivo imaging of disease-related mitochondrial dynamics in a vertebrate model system. J. Neurosci. Off. J. Soc. Neurosci 32, 16203–16212.

Polo SE, and Jackson SP (2011). Dynamics of DNA damage response proteins at DNA breaks: a focus on protein modifications. Genes Dev 25, 409–433. [PubMed: 21363960]

Prober DA, Rihel J, Onah AA, Sung R-J, and Schier AF (2006). Hypocretin/orexin overexpression induces an insomnia-like phenotype in zebrafish. J. Neurosci. Off. J. Soc. Neurosci 26, 13400–13410.

Prokocimer M, Davidovich M, Nissim-Rafinia M, Wiesel-Motiuk N, Bar DZ, Barkan R, Meshorer E, and Gruenbaum Y (2009). Nuclear lamins: key regulators of nuclear structure and activities. J. Cell. Mol. Med 13, 1059–1085. [PubMed: 19210577]

Randlett O, Wee CL, Naumann EA, Nnaemeka O, Schoppik D, Fitzgerald JE, Portugues R, Lacoste AMB, Riegler C, Engert F, et al. (2015). Whole-brain activity mapping onto a zebrafish brain atlas. Nat. Methods 12, 1039–1046. [PubMed: 26778924]

Ray Chaudhuri A, and Nussenzweig A (2017). The multifaceted roles of PARP1 in DNA repair and chromatin remodelling. Nat. Rev. Mol. Cell Biol 18, 610–621. [PubMed: 28676700]

Reichert S, Pavón Arocas O, and Rihel J (2019). The Neuropeptide Galanin Is Required for Homeostatic Rebound Sleep following Increased Neuronal Activity. Neuron 104, 370–384.e5. [PubMed: 31537465]

Rodriguez AV, Funk CM, Vyazovskiy VV, Nir Y, Tononi G, and Cirelli C (2016). Why Does Sleep Slow-Wave Activity Increase After Extended Wake? Assessing the Effects of Increased Cortical Firing During Wake and Sleep. J. Neurosci. Off. J. Soc. Neurosci 36, 12436–12447.

Rogakou EP, Pilch DR, Orr AH, Ivanova VS, and Bonner WM (1998). DNA double-stranded breaks induce histone H2AX phosphorylation on serine 139. J. Biol. Chem 273, 5858–5868. [PubMed: 9488723]

Romano SA, Pérez-Schuster V, Jouary A, Boulanger-Weill J, Candeo A, Pietri T, and Sumbre G (2017). An integrated calcium imaging processing toolbox for the analysis of neuronal population dynamics. PLoS Comput. Biol 13, e1005526. [PubMed: 28591182]

Sabia S, Fayosse A, Dumurgier J, van Hees VT, Paquet C, Sommerlad A, Kivimäki M, Dugravot A, and Singh-Manoux A (2021). Association of sleep duration in middle and old age with incidence of dementia. Nat. Commun 12, 2289. [PubMed: 33879784]

Sela Y, Krom AJ, Bergman L, Regev N, and Nir Y (2020). Sleep Differentially Affects Early and Late Neuronal Responses to Sounds in Auditory and Perirhinal Cortices. J. Neurosci. Off. J. Soc. Neurosci 40, 2895–2905.

Selby CP, and Sancar A (1990). Molecular mechanisms of DNA repair inhibition by caffeine. Proc. Natl. Acad. Sci. U. S. A 87, 3522–3525. [PubMed: 2185474]

Singh P, and Donlea JM (2020). Bidirectional Regulation of Sleep and Synapse Pruning after Neural Injury. Curr. Biol. CB 30, 1063–1076.e3. [PubMed: 32142703]

Sinha RP, and Häder D-P (2002). UV-induced DNA damage and repair: a review. Photochem. Photobiol. Sci 1, 225–236. [PubMed: 12661961]

Soltani S, Chauvette S, Bukhtiyarova O, Lina J-M, Dubé J, Seigneur J, Carrier J, and Timofeev I (2019). Sleep–Wake Cycle in Young and Older Mice. Front. Syst. Neurosci 13, 51. [PubMed: 31611779]

Sri Kantha S, Suzuki J, Hirai Y, and Hirai H (2009). Behavioral sleep in captive owl monkey (Aotus azarae) and squirrel monkey (Saimiri boliviensis). Acta Neurobiol. Exp. (Warsz.) 69, 537–544. [PubMed: 20048768]

Stanhope BA, Jaggard JB, Gratton M, Brown EB, and Keene AC (2020). Sleep Regulates Glial Plasticity and Expression of the Engulfment Receptor Draper Following Neural Injury. Curr. Biol. CB 30, 1092–1101.e3. [PubMed: 32142708]

Stoyanova T, Roy N, Kopanja D, Raychaudhuri P, and Bagchi S (2009). DDB2 (damaged-DNA binding protein 2) in nucleotide excision repair and DNA damage response. Cell Cycle Georget. Tex 8, 4067–4071.

Suberbielle E, Sanchez PE, Kravitz AV, Wang X, Ho K, Eilertson K, Devidze N, Kreitzer AC, and Mucke L (2013). Physiologic brain activity causes DNA double-strand breaks in neurons, with exacerbation by amyloid-β. Nat. Neurosci 16, 613–621. [PubMed: 23525040]

Tammaro M, Barr P, Ricci B, and Yan H (2013). Replication-dependent and transcription-dependent mechanisms of DNA double-strand break induction by the topoisomerase 2-targeting drug etoposide. PloS One 8, e79202. [PubMed: 24244448]

Thadathil N, Hori R, Xiao J, and Khan MM (2019). DNA double-strand breaks: a potential therapeutic target for neurodegenerative diseases. Chromosome Res 27, 345–364. [PubMed: 31707536]

Tononi G, and Cirelli C (2014). Sleep and the price of plasticity: from synaptic and cellular homeostasis to memory consolidation and integration. Neuron 81, 12–34. [PubMed: 24411729]

Tsouroula K, Furst A, Rogier M, Heyer V, Maglott-Roth A, Ferrand A, Reina-San-Martin B, and Soutoglou E (2016). Temporal and Spatial Uncoupling of DNA Double Strand Break Repair Pathways within Mammalian Heterochromatin. Mol. Cell 63, 293–305. [PubMed: 27397684]

Vidal AE, Boiteux S, Hickson ID, and Radicella JP (2001). XRCC1 coordinates the initial and late stages of DNA abasic site repair through protein-protein interactions. EMBO J 20, 6530–6539. [PubMed: 11707423]

Wagner N, and Krohne G (2007). LEM-Domain proteins: new insights into lamin-interacting proteins. Int. Rev. Cytol 261, 1–46. [PubMed: 17560279]

Weber F, and Dan Y (2016). Circuit-based interrogation of sleep control. Nature 538, 51–59. [PubMed: 27708309]

Xie L, Kang H, Xu Q, Chen MJ, Liao Y, Thiyagarajan M, O'Donnell J, Christensen DJ, Nicholson C, Iliff JJ, et al. (2013). Sleep drives metabolite clearance from the adult brain. Science 342, 373–377. [PubMed: 24136970]

Yokogawa T, Marin W, Faraco J, Pézeron G, Appelbaum L, Zhang J, Rosa F, Mourrain P, and Mignot E (2007). Characterization of sleep in zebrafish and insomnia in hypocretin receptor mutants. PLoS Biol 5, e277. [PubMed: 17941721]

Zada D, and Appelbaum L (2020). Behavioral criteria and techniques to define sleep in zebrafish. In Behavioral and Neural Genetics of Zebrafish, (Elsevier), pp. 141–153.

Zada D, Bronshtein I, Lerer-Goldshtein T, Garini Y, and Appelbaum L (2019). Sleep increases chromosome dynamics to enable reduction of accumulating DNA damage in single neurons. Nat. Commun 10.

Zhdanova IV, Wang SY, Leclair OU, and Danilova NP (2001). Melatonin promotes sleep-like state in zebrafish. Brain Res 903, 263–268. [PubMed: 11382414]

Zadaet al. 2021. Mol. Cell

Highlights

1. Neuronal DNA damage triggers sleep.
2. Sleep increases DNA repair and reduces cellular homeostatic pressure.
3. Activity of the DNA damage detector Parp1 increases with sleep deprivation.
4. Parp1 activity promotes sleep, chromosome dynamics, and DNA repair.

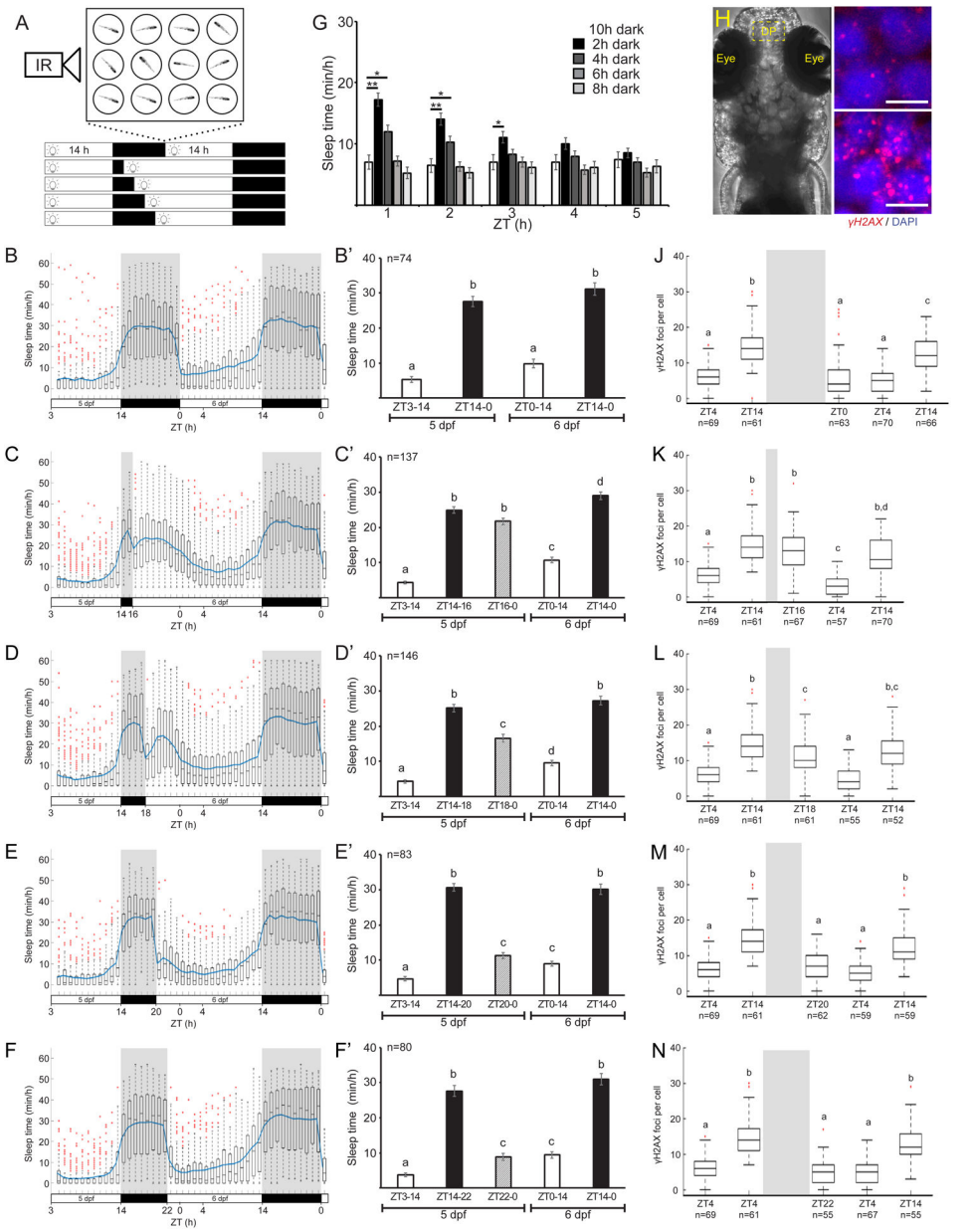

Figure 1. Six hours of consolidated sleep are sufficient to normalize neuronal DNA damage.

A. Schematic illustration of the experimental procedure. Sleep was monitored under various light/dark regimes. **B-F'.** Sleep of 5–6 dpf larvae under an 14 h light/ 10 h dark cycle (**B, B'**, $p = 8\times10^{-40}$), 14 h light/ 2 h dark cycle (**C, C',** $p = 3\times10^{-94}$), 14 h light/ 4 h dark cycle (**D, D',** $p = 4\times10^{-66}$), 14 h light/ 6 h dark cycle (**E, E'**, $p = 1\times10^{-83}$), 14 h light/ 8 h dark cycle (**F, F'**, $p = 2\times10^{-59}$). The bar charts represent the average sleep time for each time bin. **G.** Average sleep time of all groups in the first 5 h of the 2nd day. $*p < 0.05$, $**p < 0.01$, two-tailed *t*-test: two samples assuming unequal variance. **H.** Dorsal view of 6 dpf larvae. Dashed box showing the dorsal pallium (DP) area analyzed in **J-N**. **I.** Representative neuron nuclei stained with DAPI and γH2AX in the DP during the morning (ZT4) and the end of the day (ZT14). Scale bar = 5 μm. **J-N.** The levels of DNA damage in single neuronal nuclei

over 34 h. All time points were compared to the baseline levels of the first day (5 dpf). **J**. 14 h light/10 h dark cycle, $p = 1.9\times10^{-35}$. **K.** 14 h light/ 2 hr dark cycle, $p = 1.8\times10^{-39}$. **L.** 14 h light/ 4 h dark cycle, $p = 2.2\times10^{-33}$. **M.** 14 h light/ 6 h dark cycle, $p = 8.1\times10^{-38}$. **N.** 14 h light/ 8 h dark cycle, $p = 4.5\times10^{-44}$. Letters indicate significant differences ($p < 0.05$), one-way ANOVA followed by Tukey's test (**B'-F', J-N)**. Data show means ± SEM (**B'-F', G**) or boxplots (**B-F, J-N**). Blue line represents mean. Red crosses indicate outliers. n=number of animals (**B'-F'**) or cells (**J-N**). ZT–zeitgeber time.

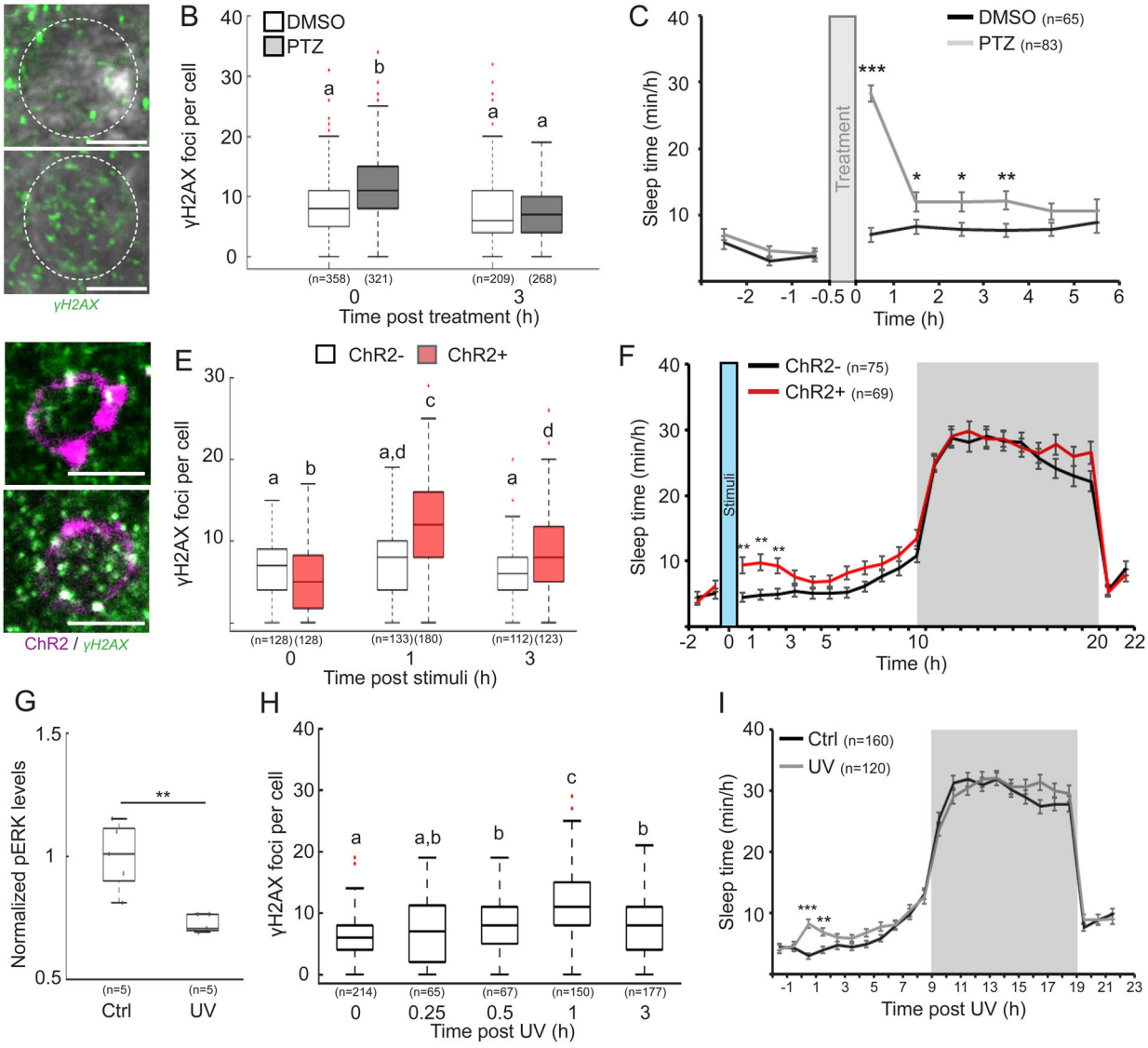

Figure 2. Neuronal activity- and UV-induced DNA damage promote sleep.

A. Representative images of γH2AX staining in neurons of the DP region of 6 dpf larvae immediately following 30 min of DMSO or PTZ treatment. Dashed circle indicates a single neuron. **B.** The levels of DNA damage in single nuclei immediately (0) and 3 h following DMSO or PTZ treatment. $p = 1.3\times10^{-9}$. **C.** Sleep before and after PTZ treatment in 6 dpf larvae. **D.** Representative images of γH2AX staining (green) in the DP region of *tg(HuC:Gal4/uas:ChR2-mCherry)* 6 dpf larvae expressing *ChR2-mCherry* (magenta) immediately and 1 h following 10 min of blue light stimuli. **E.** The levels of DNA damage in single neuronal nuclei. $p = 2\times10^{-20}$. **F.** Sleep before and after 10 min of blue light stimuli in 6 dpf *tg(HuC:Gal4)/tg(uas:ChR2-mCherry)* (ChR2−) and *tg(HuC:Gal4/uas:ChR2-mCherry)* (ChR2+) larvae. **G.** Levels of α-pERK in the DP of 6 dpf larvae following 2 min exposure to purple (Ctrl) or UV light. **H.** The levels of DNA damage in single nuclei following 2 min UV exposure. $p = 4.4\times10^{-28}$. **I.** Sleep prior and post 2 min exposure to ctrl or UV light. Data show mean ± SEM (**C, F, I**), or boxplots (**B, E, G, H**). Red crosses indicate outliers. *$p <$

0.05, $**p < 0.01$, $***p < 0.001$. Letters indicate significant differences ($p < 0.05$), two-tailed *t*-test: two samples assuming unequal variance (**C, F, G, I**), one-way (**H**) or two-way (**B, E**) ANOVA followed by Tukey's test. n=number of animals (**C, F, G, I**) or cells (**B, E, H**). Scale bar = 5 μm.

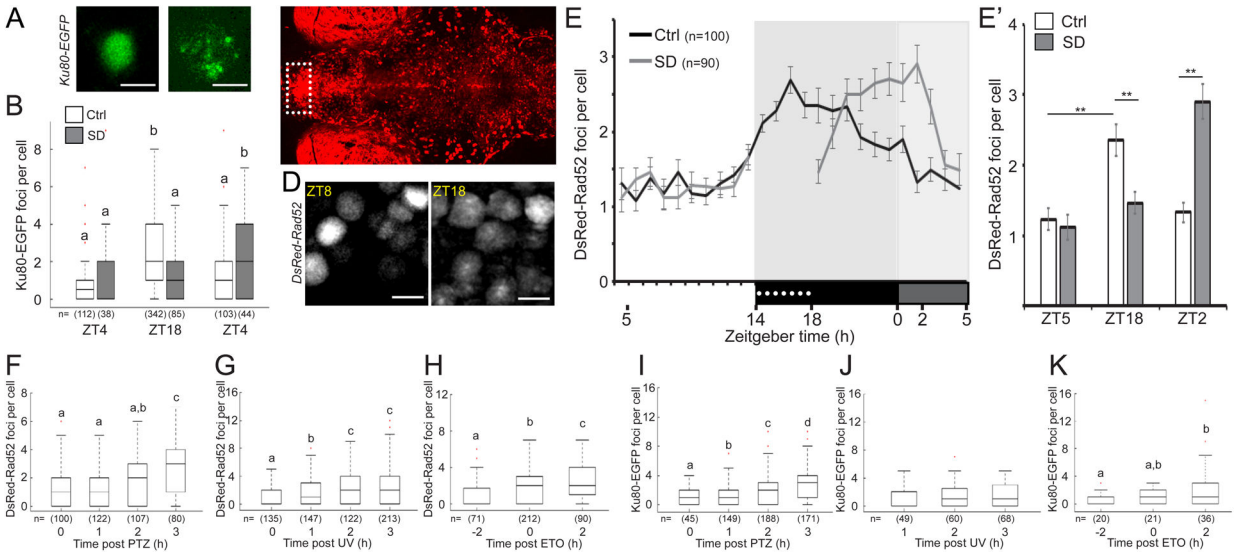

Figure 3. Rad52- and ku80-repair activity is increased during sleep and post induction of DNA damage.

A. Representative images of *HuC*-driven Ku80-EGFP expression in neuron of 6 dpf larvae during day (ZT4) and night (ZT18). **B.** Number of Ku80-EGFP foci in single neurons under LD to constant darkness (LDD). p=1.1×10^{-16}. **C.** Dorsal view of 6 dpf *tg(HuC:Gal4/uas:DsRed-Rad52)* larvae. Dashed box marks the dorsal pallium (DP). MB- midbrain. **D.** Representative images of the same DP region of 6 dpf *tg(HuC:Gal4/uas:DsRed-Rad52)* larvae during day (ZT8) and night (ZT18). **E, E'.** The number of DsRed-Rad52 foci in single neurons of the DP under LDD. **p < 0.01, two-tailed t-test: two samples assuming unequal variance. **F-H.** The number of DsRed-Rad52 foci in single nuclei following 30 min of PTZ treatment (**F**, p = 4.2×10^{-12}), following 2 min UV exposure (**G**, p = 1.9×10^{-12}), and before, immediately after, and following ETO treatment (**H**, p = 3.3×10^{-9}). **I-K.** The number of Ku80-EGFP foci in single nuclei following 30 min of PTZ treatment (**I**, p = 3.6×10^{-13}), following 2 min UV exposure (**J**), and before, immediately after, and following ETO treatment (**K**, p = 0.03). Data show mean ± SEM (**B, E, E'**), or boxplots (**F-K**). Red crosses indicate outliers. Letters indicate significant differences (p < 0.05), one-way (**F-K**) or two-way (**B, E'**) ANOVA followed by Tukey's test. n-number of cells. ZT–zeitgeber time. Scale bar = 5 μm.

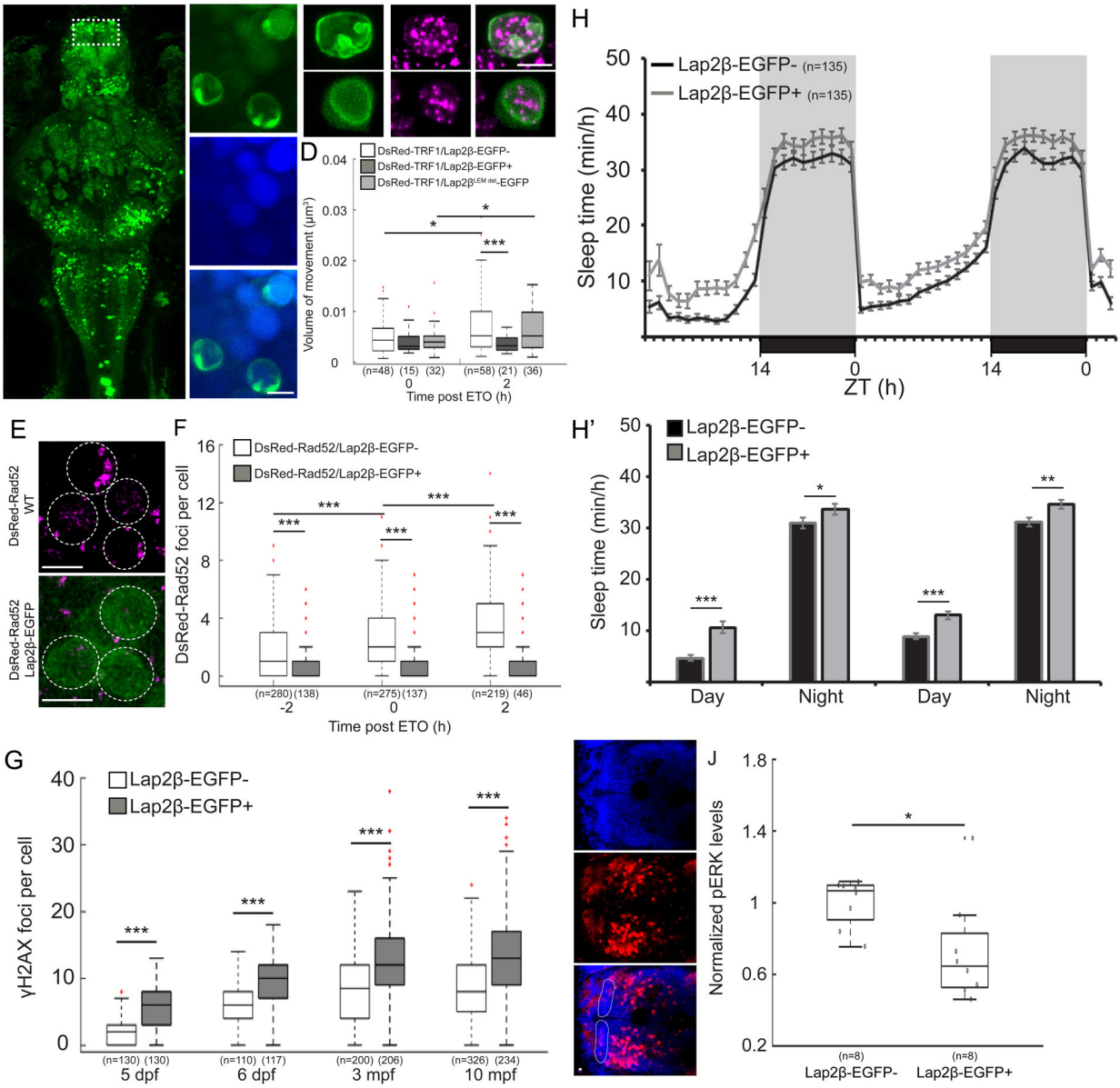

Figure 4. Inhibition of chromosome dynamics reduces Rad52-repair activity and increases DNA damage and compensatory sleep.

A. Dorsal view of 6 dpf *tg(HuC:Gal4/uas:Lap2β-EGFP)* larvae (Lap2β-EGFP+). Dashed box shows the dorsal pallium (DP). MB- midbrain, Rh- rhombencephalon. **B.** Representative image of Lap2β-EGFP expression in the nuclei. **C.** Co-expression of Lap2β-EGFP (green, upper panel) or Lap2β^{LEMdel}-EGFP (green, lower panel) and chromosome marker (DsRed-TRF1, magenta) in the nucleus of DP neurons. **D.** Volume of chromosome dynamics during 5 min in neurons of the DP immediately and 2 h after ETO treatment. **E.** Neurons of the DP that express either DsRed-Rad52 or both DsRed-Rad52 and Lap2β-EGFP. **F.** The number of DsRed-Rad52 foci in the DP of 6 dpf larvae 2 h before, immediately after, and 2 h after ETO treatment. **G.** The levels of DNA damage in larvae and adult brains. **H. H'.** Sleep of 5–6 dpf larvae under a 14 h light/ 10 h dark cycle. **H'**. The average sleep time during

the day and the night. **I.** Dorsal view (head points to the left) of the brain of 6 dpf larvae stained with α-pERK (red) and DAPI (blue). Dashed area marks the DP**. J**. Average pERK expression in single neurons of the DP of 6 dpf siblings. $*p < 0.05$, $**p < 0.01$, $***p < 0.001$, two-tailed *t*-test: two samples assuming unequal variance (**D, G-J**), two-way ANOVA followed by Tukey's test (**F**). Data show mean ± SEM (**H, H'**), or boxplots (**D, F, G, J**). Red crosses indicate outliers. n=number of animals (**H, J**) or cells (**D, F, G**). ZT-zeitgeber time. Scale bar = 5 μm.

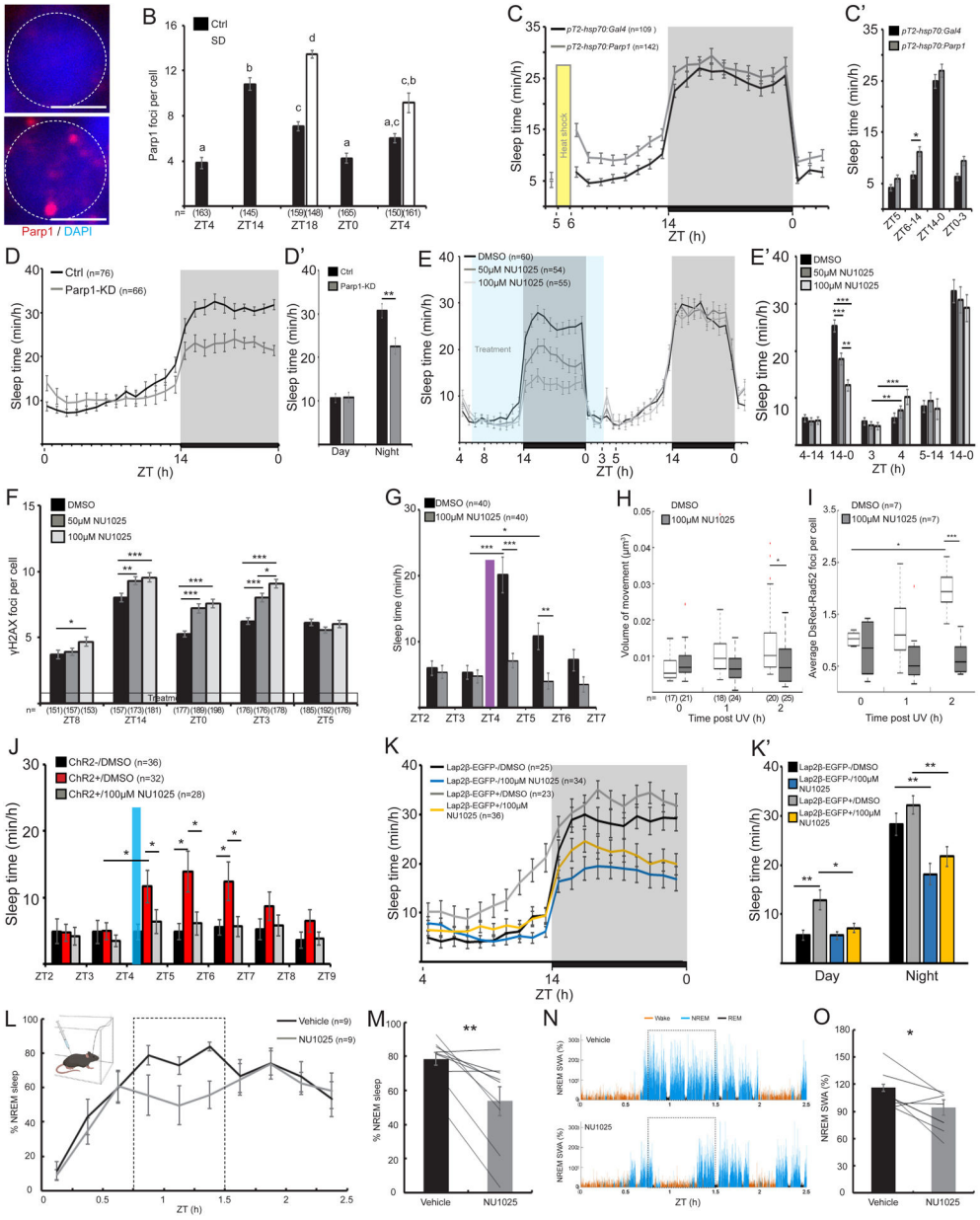

Figure 5. Parp1 regulates DNA damage-induced sleep.

A. Representative nuclei in DP neuron stained with DAPI and α-Parp1 at ZT4 and at the end of the day (ZT14). Dashed circle indicates a single neuron. Scale bar = 3 μm. **B.** The number of Parp1 foci in single DP neuronal nuclei. Letters indicate significant differences ($p < 0.05$). **C.** Sleep of 6–7 dpf *pT2-hsp70:Parp1*-injected and control *pT2-hsp70:Gal4*-injected larvae, before and following heat shock (see Figure S5C for Parp1 expression levels). **C`.** The average sleep time during portions of daytime and entire nighttime. **D.** Sleep of 6 dpf Parp1-KD larvae and their Ctrl siblings under a 14 h light/ 10 h dark cycle (see Figure S5C for Parp1 expression levels). **D'**. The average sleep time during the day and the night. **E.** Sleep of 5–6 dpf larvae under a 14 h light/ 10 h dark cycle, before, during (blue box), and following treatment with DMSO, 50 μM or 100 μM of the Parp1 inhibitor NU1025.

È. The average sleep time during portions of daytime and entire nighttime. **F.** The number of γH2AX foci. **G-I.** Sleep time (**G**), chromosome dynamics in neurons of the DP (**H,** boxplots) and the average number of DsRed-Rad52 foci per larvae (**I,** boxplots) in 6 dpf DMSO- or NU1025-treated larvae before and following 2 min of UV radiation. **J.** Sleep of 6 dpf larvae before and following 10 min of blue light (480 nm) stimuli. **K. K'.** Sleep of 6 dpf Lap2β-EGFP+ and Lap2β-EGFP− siblings with either DMSO or 100 μM NU1025, under a 14 h light/ 10 h dark cycle. **K'**. The average sleep time during the day and night. **L-O**. Validation of the role of Parp1 in adult mice. **L**. Time course of percent time in NREM sleep in ZT0–2.5h after injection of parp1 inhibitor NU1025 or vehicle. Dashed rectangle marks the 0.75–1.5 h time interval used for quantitative comparison in **M**. Illustration embedded in top left depicts setup schematics. **M**. Percent time in NREM in individual subjects. **N**. Representative examples of frontal EEG slow wave activity (SWA) in ZT0–2.5 h (% of average NREM SWA per minute in baseline saline session of each animal) after injection of vehicle (top) and NU1025 (bottom) in the same subject. Dashed rectangle marks the 0.75–1.5 h time interval used for quantitative comparison in **O**. **O**. NREM SWA in individual subjects. Data show mean ± SEM. Lines (**M**, **O**) represent individual mouse data. $*p < 0.05$, $**p < 0.01$, $***p < 0.001$. Two-tailed *t*-test: two samples assuming unequal variance (**C', D', E', F, G, J, K'**), one-way (**B**), two-way (**H, I**) ANOVA followed by Tukey's test, one-tailed sign-rank test (**M, O**). n-number of animals (**C-E, G, J-L**) or cells (**B, F, H, I**). ZT-zeitgeber time.

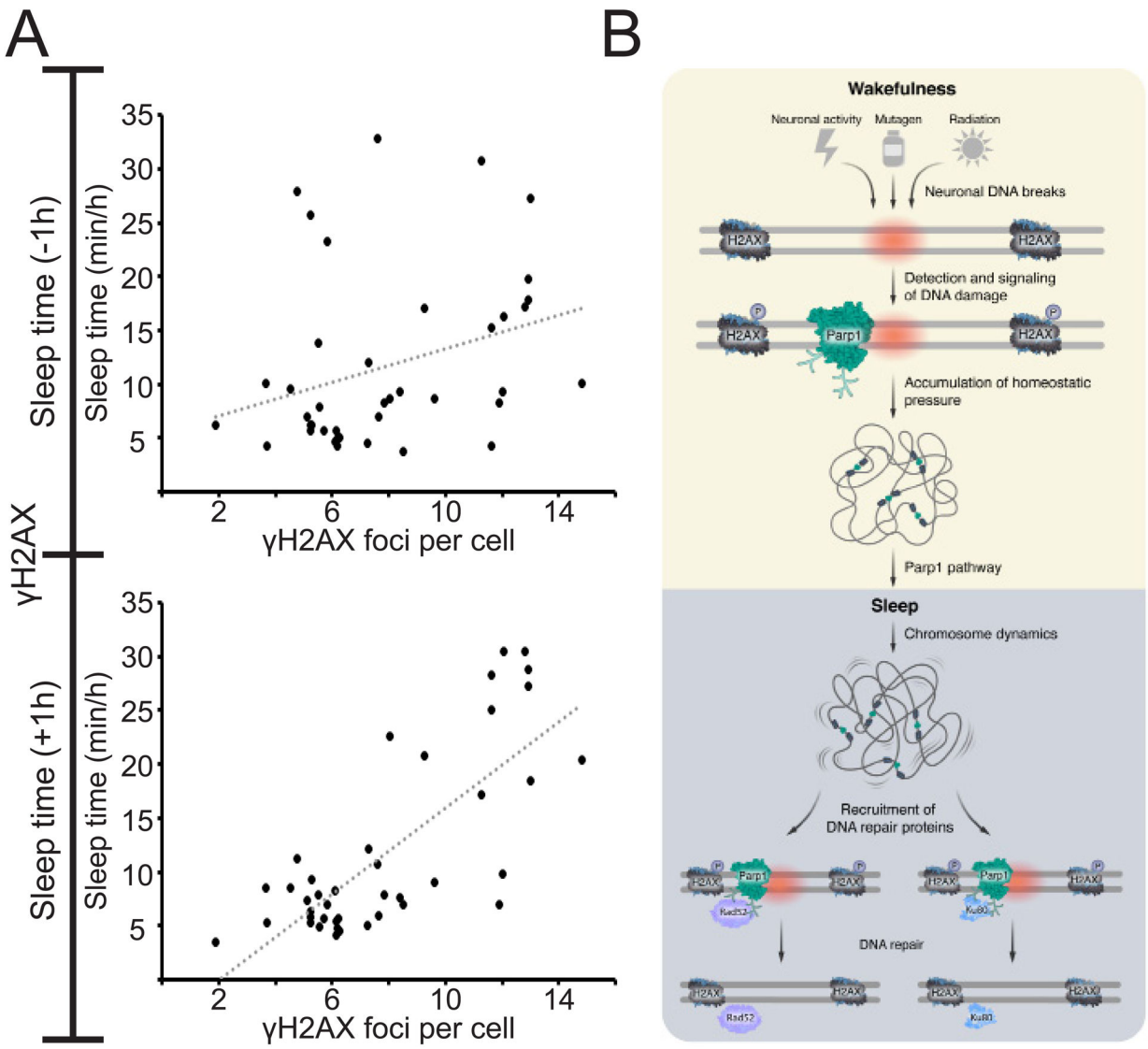

Figure 6. Proposed cellular mechanism for homeostatic regulation of sleep.

A. Plots of sleep time and γH2AX foci number (collection of data presented in Figures 1–5). Weak correlation ($R = 0.3$) between the amount of DNA damage and sleep time prior to the quantification of γH2AX foci (upper graph). Strong positive correlation ($R = 0.76$) between the amount of DNA damage and sleep time following the quantification of γH2AX foci (lower graph). This correlation suggests that the amount of the homeostatic driver – DNA damage – can predict the requirement of sleep time. Pearson correlation coefficient.

B. During wakefulness, various processes, ranging from neuronal activity and radiation to mutagen activity, cause DNA damage in neurons (red circle). The DNA damage detector Parp1 is immediately recruited and activated in DNA loose ends, and soon after, the H2AX histone is phosphorylated (p). The accumulation of DNA damage is a homeostatic driver for sleep, and Parp1 activity and downstream pathways can mediate the signal to sleep. During sleep, chromosome dynamics increase, which enables the recruitment and efficient activity of the repair proteins Rad52 and Ku80 and their repair signaling pathways. Then,

Parp1 is deactivated, the number of γH2AX is reduced, and the DNA damage-dependent homeostatic pressure to sleep is relieved. The duration and efficiency of this process may explain species-specific length and quality of sleep and repair (6 h in zebrafish larvae).

KEY RESOURCES TABLE

REAGENT or RESOURCE	SOURCE	IDENTIFIER
Antibodies		
Rabbit anti-γH2AX	GeneTex	GTX127342; RRID:AB_2833105
Rabbit anti Phospho-p44/42 MAPK (Erk1/2)(Thr202/Tyr204)	Cell Signaling Technology	CST-4370S; RRID:AB_2895021
Goat anti-rabbit IgG H&L (Alexa FluorTM 594)	Invitrogen	A11012; RRID:AB_141359
Goat anti-rabbit IgG H&L (Alexa FluorTM 488)	Invitrogen	A11008; RRID:AB_143165
DAPI/Antifade (250 ng/ml) counterstain	Santa Cruz Biotechnology	sc-3598
Parp1 Antibody	Abcam	ab194586; RRID:AB_2895023
Anti-GAPDH Antibody (0411)	Santa Cruz Biotechnology	sc-47724; RRID:AB_627678
Chemicals, Peptides, and Recombinant Proteins		
Etoposide (ETO)	SIGMA-ALDRICH	E1383
NU1025	SIGMA-ALDRICH	N7287
Pentylenetetrazole (PTZ)	SIGMA-ALDRICH	P6500
Dimethyl Sulfoxide (DMSO)	SIGMA-ALDRICH	D8418
Paraformaldehyde (PFA), prills, 95%	SIGMA-ALDRICH	441244
Polyethylene glycol 200 (PEG-200)	SIGMA-ALDRICH	8.07483
Dulbecco's Phosphate Buffered Saline (PBS), 10X Conc., without Calcium and Magnesium	Biological Industries	02-023-5A
Fetal Bovine Serum (FBS)	Biological Industries	041271A
Alt-R® S.p. Cas9 Nuclease V3, 100 µg	IDT	1081058
Experimental Models: Organisms/Strains		
Zebrafish: *tg(HuC:Gal4)*	(Plucińska et al., 2012)	N/A
Zebrafish: *tg(dbh:Gal4)*	Current work	N/A
Zebrafish: *tg(fli1:EGFP)*	(Lawson and Weinstein, 2002)	N/A
Zebrafish: *tg(sox10:EGFP)*	ZFIN	ZDB-TGCONSTRCT-150414-3
Zebrafish: *tg(uas:DsRed-Rad52)*	Current work	N/A
Zebrafish: *tg(uas:DsRed-TRF1)*	Current work	N/A
Zebrafish: *tg(HuC:GCaMP5)*	(Romano et al., 2017)	N/A
Zebrafish*: tg(ChR2-mCherry)*	(Helmbrecht et al., 2018)	N/A
Zebrafish: *tg(uas:Lap2β-EGFP)*	Current work	N/A
Mice: C57BL/6j	Envigo/ in house breeding	N/A
Oligonucleotides		
Primers for cloning and RT-PCR (Methods details)	Current work	N/A
sgRNA list (Method details)	Current work	N/A
Recombinant DNA		
Plasmid: *pT2-uas:DsRed-Rad52*	Current work	N/A
Plasmid: *pT2-uas:dsRed-Rad52*^{R49A}	Current work	N/A
Plasmid: *pT2-uas:Ku80-EGFP*	Current work	N/A

REAGENT or RESOURCE	SOURCE	IDENTIFIER
Plasmid: *pT2-uas:ku80$^{D721A/D722A}$-EGFP*	Current work	N/A
Plasmid: *pT2-uas:Lap2β-EGFP*	(Zada et al., 2019)	N/A
Plasmid: *pT2-uas:Lap2β^{LEMdel}-EGFP*	Current work	N/A
Plasmid: *pT2-hsp70:Parp1*	Current work	N/A
Software and Algorithms		
EthoVision XT 12 software	Noldus Information Technology	N/A
MATLAB	Mathworks	https://www.mathworks.com/products/matlab.html
Imaris	Oxford Instruments	N/A
ImageJ	NIH imageJ	https://imagej.nih.gov/ij/
Excel	Microsoft	https://office.microsoft.com/excel/
Other		
Noldus DanioVision tracking system	Noldus Information Technology	N/A
CFX96™ Real-Time PCR	BIO RAD	N/A
Direct-zol RNA MiniPrep kit	Zymo Research Corporation	ZR-R2051
qScript cDNA SuperMix	Quanta BioSciences	95047
PerfeCTa SYBR Green FastMix	Quanta BioSciences	95073
Comet assay kit	Abcam	ab238544